DOI: 10.26599/FSHW.2026.9251134

Contents lists available at SciOpen

Food Science and Human Wellness

journal homepage: https://www.sciopen.com/journal/2097-0765

China Food Publishing Co.

Gastrodia elata polysaccharides ameliorate gastric mucosal injury by driving metabolic homeostasis and activating the PI3K/Rac1 signaling axis

Mengsi Guo[1,2#], Shaoqi Pu[1,2#], Guannan Hu[1,2], Ziyun Hu[1,2], Wenya Liu[1,2], Di Xu[1,2]*, Junsong Wang[1,2]*

[1]*Center for Molecular Metabolism, School of Environmental and Biological Engineering, Nanjing University of Science and Technology, Nanjing 210094, China.*

[2]*Key Laboratory of Metabolic Engineering and Biosynthesis Technology, Ministry of Industry and Information Technology, Nanjing University of Science and Technology, Nanjing 210094, China.*

ABSTRACT: Gastric mucosal injury represents a critical risk factor for gastric cancer development, with pathogenesis involving *Helicobacter pylori* infection, alcohol consumption, and nonsteroidal anti-inflammatory drugs. Conventional synthetic drug therapies offer incomplete relief with side effects, underscoring the need for alternatives like food-medicine homologous substances. *Gastrodia elata* polysaccharides (GEP), the primary active components of the food-medicine homologous plant, exhibit antioxidant and anti-inflammatory potential. However, their therapeutic mechanisms against gastric injury remain incompletely elucidated. This study aimed to investigate the protective effects and mechanisms of GEP on ethanol-induced acute gastric mucosal injury in rats. Results demonstrated that medium-dose crude GEP (GEP-M) and purified GEP (GBP) most effectively ameliorated gastric mucosal injury. GEP-M and GBP treatment modulated gastrointestinal microbiota, increasing the abundance of probiotics (e.g., *Lactobacillus* and *Bifidobacterium*) while reducing pathogenic bacteria (e.g., *Helicobacter*, *Escherichia-Shigella*, and *Streptococcus*). Untargeted gastric metabolomics identified 61 significantly altered metabolites, primarily enriched in the TCA cycle, glycolysis, tryptophan metabolism, and steroid hormone biosynthesis. Changes in probiotic and pathogenic bacterial abundances were strongly correlated with shifts in metabolites involved in tryptophan metabolism and steroid hormone biosynthesis. To further investigate the functional link between differentially metabolites and signaling pathways, we constructed a metabolite–gene interaction network, which revealed 94 key genes directly associated with these differential metabolites. Intersection analysis between these metabolite-targeted genes and genes strongly associated with gastric mucosal injury yielded 31 candidate genes. Subsequent expression level validation of these candidates confirmed the activation of the PI3K/Rac1 signaling pathway after GEP treatment. Collectively, these findings suggest that GEP may ameliorate gastric mucosal injury by driving metabolic homeostasis and activating the PI3K/Rac1 signaling axis, highlighting the potential of natural polysaccharides as promising therapeutic agents for gastric diseases.

Keywords: *Gastrodia elata* polysaccharides, gastric mucosal injury, gastrointestinal microbiota, metabolomics, PI3K/Rac1

1. Introduction

[#]Mengsi Guo and Shaoqi Pu contributed equally to this work
***Corresponding author**
Di Xu, xudi@njust.edu.cn
Junsong Wang, wangjunsong@njust.edu.cn

Received 1 December 2025
Received in revised from 26 December 2025
Accepted 10 March 2026

Gastric mucosal injury (GMI) represents a significant global health challenge, manifesting clinically as dyspepsia, epigastric pain, and, in acute phases, life-threatening gastrointestinal hemorrhage[1,2]. If not promptly repaired, GMI can progress to gastric ulcers, a common digestive disease that affects approximately 10% of the global population[3]. More concerning is that sustained gastric mucosal injury significantly elevates the risk of progressing to gastric cancer[4]. While traditional culprits like *Helicobacter pylori* (*H. pylori*) infection, excessive alcohol consumption, and chronic nonsteroidal anti-inflammatory drugs (NSAIDs) use remain primary drivers of mucosal erosion[5–8], emerging paradigms emphasize the gastric microenvironment. Recent evidence suggests that the pathogenesis of GMI is not merely a result of acid-pepsin aggression but is deeply intertwined with gut microbiota dysbiosis[9–11]. Patients with these conditions often exhibit reduced diversity of the gut microbiota, along with an increased abundance of certain pathogenic bacterial species[12]. While a breakdown in microbial homeostasis often precedes mucosal structural failure, the underlying metabolic signaling pathways remain unclear. In particular, the exact mechanisms by which microbial metabolites influence host cellular repair have yet to be fully elucidated.

Current pharmacological interventions, primarily dominated by proton pump inhibitors (PPIs) and H2-receptor antagonists, focus heavily on acid suppression[13]. Despite their efficacy, long-term reliance on these agents is limited by adverse effects, including acid rebound, increased susceptibility to enteric infections, and impaired mucosal healing. Consequently, there is an urgent need for safe and non-toxic therapeutic strategies that offer multitargeted protection rather than simple acid neutralization. Bioactive compounds derived from food and medicine homology sources have emerged as promising candidates due to their high efficacy and minimal systemic toxicity[14–16]. Previous studies have shown that polysaccharides derived from the fruiting bodies of *Hericium erinaceus* significantly attenuate ethanol-induced gastric mucosal injury and pylorus ligation-induced ulcers[17,18]. While these studies highlighted broad anti-inflammatory and antioxidant properties, the specific regulatory role of these polysaccharides in modulating intracellular metabolic signaling axis remains largely unexplored.

Gastrodia elata (*G. elata*), a traditional medicinal plant belonging to the Orchidaceae family, was formally integrated into the national “Food and Medicine Homology” catalog in 2020[19,20]. Among its bioactive compounds, *G. elata* polysaccharides (GEP), have emerged as primary functional components characterized by their immunomodulatory and anti-inflammatory properties. For instance, Guan et al. found that *G. elata* polysaccharides can stimulate macrophages to release nitric oxide (NO), enhance phagocytic activity, and exhibit dose-dependent immune regulatory functions at the cellular level[21]. Building upon our previous research, Chen et al. demonstrated that aqueous extracts of *G. elata* effectively suppressed gastric

inflammation and reversed the metabolic dysregulation in chronic atrophic gastritis[22]. In our subsequent work, we identified GEP as a primary bioactive constituent of aqueous extracts, demonstrating its capacity to significantly attenuate inflammatory bowel disease (IBD) symptoms in mice[23]. These therapeutic outcomes were closely linked to the improvement of gut microbiota composition and its associated metabolic profiles. However, despite these preliminary findings, the specific molecular orchestration between microbial metabolites and host cellular repair remains elusive. In this study, we aim to bridge this gap by investigating whether GEP can preserve mucosal integrity through the restoration of microbial homeostasis and the subsequent activation of the PI3K/Rac1 axis which is essential for epithelial cytoskeletal reorganization and cell migration. By constructing a metabolite–gene interaction network, we seek to provide a comprehensive mechanistic framework that defines the potential genetic targets and metabolic drivers underlying GEP-mediated gastroprotection.

2. Materials and methods

2.1 Materials and reagents

Dried rhizomes of *G. elata* (originating from Zhaotong, Yunnan) were obtained from Yunnan Manji Biotechnology Co., Ltd. (Yunnan, China). Dialysis bags (MD55) were sourced from Solarbio (Beijing, China). Anhydrous ethanol was purchased from Sinopharm Chemical Reagent Co., Ltd. (Shanghai, China), and 4% neutral-buffered formaldehyde was obtained from Servicebio (Wuhan, China). Biochemical assay kits for superoxide dismutase (SOD, A001-3), glutathione (GSH, A006-2-1), malondialdehyde (MDA, A003-1), nitric oxide (NO, A013-2-1), prostaglandin E_2 (PGE_2, H099-1-1), and epidermal growth factor (EGF, H031-1-1) were supplied by the Nanjing Jiancheng Bioengineering Institute (Nanjing, China). For molecular analysis, Trizol reagent was purchased from Gibco (Grand Island, NY, USA), and the SYBR Green Premix Ex Taq II Kit was obtained from Takara Biomedical Technology (Beijing, China). Protein analysis reagents, including the BCA Protein Quantification Kit were purchased from Yeasen Biotechnology (Shanghai, China). the Active Rac1/Cdc42 Pull-down and Detection Kit and the primary antibody against Rac1 were acquired from Thermo Fisher Scientific (MA, USA). Other primary antibodies, including p-AKT, AKT, and β-actin, as well as anti-mouse and anti-rabbit secondary antibodies, were obtained from Proteintech (Wuhan, China). Antibodies against Cdc42 and β-catenin were purchased from Abways (Shanghai, China).

2.2 Polysaccharides preparation

The crude *G. elata* polysaccharides (GEP) and purified *G. elata* polysaccharides (GBP) were prepared from the fruiting bodies using a water-extraction and ethanol precipitation methods, following previously established procedures[23].

2.3 Effect of GEP against ethanol-induced gastric mucosal injury

2.3.1 Animal experiment design

A total of 56 adult male Sprague Dawley rats (180-220 g) were purchased from the Qinglongshan Laboratory Animal Center Company (Nanjing, China). All animal care and experimental procedures were conducted in strict accordance with the guidelines approved by the Institutional Animal Care and Use Committee at Nanjing University of Science and Technology (ACUC-NJUST-202100126). The rats were housed in standard cages in a room with a controlled experimental condition at 25 ± 1 ℃ and 50 ± 10% humidity under a 12 h light-dark cycle with ad libitum access to food and water. Referring to previous studies[17,23], after a one-week adaptation period, the rats were randomly divided into seven groups (Fig. 1A) (n = 8 per group): (1) control group (CON); (2) ethanol-induced model group (MOD); (3) GEP low-dose group (GEP-L, 100 mg/kg); (4) GEP medium-dose group (GEP-M, 200 mg/kg); (5) GEP high-dose group (GEP-H, 400 mg/kg); (6) GBP medium-dose group (GBP, 200 mg/kg); (7) positive control group treated with omeprazole (OMZ, 20 mg/kg). The CON and MOD groups received an equivalent volume of normal saline (0.9% NaCl), while the treatment groups were administered their respective doses of polysaccharides or omeprazole once daily via oral gavage for 14 consecutive days. On day 15, all rats were fasted for 24 h but had free access to water. The body weights were recorded before and after the experiment period. One hour after oral administration on day 15, all groups except the CON group were given 1 ml of absolute ethanol by gavage to induce acute gastric mucosal injury. The rats were anesthetized with 1.5%-2.0% isoflurane after 1 h. Blood, fecal and stomach samples were collected for further analysis.

2.3.2 Gastric macroscopic evaluation, ulcer inhibition rate and gastric juice pH

After euthanasia, the stomachs were rapidly excised, opened along the greater curvature, and gently rinsed with normal saline to remove gastric contents. The gastric mucosa was carefully examined for macroscopic damage. The number of hemorrhagic spots was recorded, and the length and width of ulcer stripes were measured with a vernier caliper. The ulcer index was calculated applying the GUTH method[24], and the scoring criteria were listed in Table S1. The ulcer inhibition rate was calculated using the following formula:

Ulcer inhibition (%) = $[(A_0-A_1)/A_0]\times100$

Where A_0 is the lesion index of the MOD group, A_1 is the lesion index of the treatment group.

After excision of the stomach along the greater curvature, the gastric contents were centrifuged at 3,000 × g for 10 min at 10 °C. The supernatant was collected, and pH was measured with an FE-28 pH meter (Mettler Toledo FiveEasy Plus, Shanghai, China).

2.4 Histopathology

For histopathology, the stomach, after being washed with normal saline, was fixed in 4% neutral-buffered formaldehyde for 24 h and then embedded in paraffin. Serial thin sections of 4-5 μm were sliced and stained with hematoxylin eosin (HE) and Alcian blue-Periodic acid Schiff (AB-PAS). The histopathological changes in the gastric mucosa of rats were observed under a light microscope (Nikon, Tokyo, Japan).

2.5 Gastrointestinal microbiota analysis by 16S rRNA gene sequencing

Total DNA was extracted from the fecal samples, and primers targeting conserved regions of the 16S rRNA gene were designed with attached sequencing adapters for PCR amplification. The amplicons were purified, quantified, and homogenized to construct a sequencing library. The library preparation was constructed using the TruSeq® DNA PCR-Free Sample Preparation Kit and quantified by Qubit and Q-PCR[23]. After quality assessment, the library was sequenced on a NovaSeq 6000 (Beijing Novogene Bioinformation Science and Technology Co., Ltd., Beijing, China). Raw sequencing reads were processed using FLASH (version 1.2.11, http://ccb.jhu.edu/software/FLASH/) to merge paired-end reads based on overlapping barcode and adapter sequences. All valid tags were clustered into operational taxonomic units (OTUs) using the Uparse algorithm with a 97% sequence similarity cutoff. Taxonomic annotation of OTUs was performed using the SILVA138 SSUrRNA database and the Mothur method. Alpha diversity indices, including Observed_species (OS), Shannon, Pielou_evenness were calculated using QIIME software (version 1.9.1, https://qiime.org/install/install.html). The differences in the relative abundances of the gut microbiota between groups were compared by analysis of similarities (ANOSIM) and LEfSe software (version 1.0). Given the distribution characteristics of the microbial taxonomic abundance and the sample size (n=6), outlier detection analysis was performed using the boxplot method based on the interquartile range (IQR).

2.6 Metabolomics profiling

2.6.1 Sample preparation

Gastric tissue samples were homogenized in a pre-chilled MeOH/H_2O (V/V = 4:1) mixture at a ratio of 30 μL/mg. After incubating at -20 °C for 1 h, the homogenates were centrifuged at 16,000 × g for 15 min at 4 °C. A volume of 400 μL of the supernatant was collected from each sample, and 100 μL from each was pooled to prepare the quality control (QC) group. The collected supernatants were dried using nitrogen gas and further lyophilized. The dried sample were resuspended in 150 μL of MeOH/H_2O (V/V = 1:1), vortex for 30 s, and sonicated for 1 min in an ice-water bath. Subsequently, the samples were centrifuged again at 16,000

× g for 15 min at 4 °C. The resulting supernatants were transferred into UHPLC vials and subjected to UHPLC-QTOF-MS analysis.

2.6.2 UHPLC-QTOF-MS analysis

UHPLC-QTOF-MS analysis was performed using a Triple TOF 5600$^+$ mass spectrometer (AB Sciex, Framingham, MA, USA) equipped with a Phenomenex Kinetex® C18 column (100 × 2.1 mm, 2.6 μm, Waters Corporation, Milford, MA, USA) with a guard column (Security Guard UHPLC C18 column). Qualitative analysis was performed in IDA mode. Mobile phase A was 0.1% formic acid in water, and mobile phase B was acetonitrile, with an injection volume of 10 μL for both. Elution was performed using the following gradient at a flow rate of 0.4 mL/min: 0 min, 1% B; 1 min, 1% B; 10 min, 99% B; 13 min, 99% B; 14 min, 1% B; 17 min, 1% B. Mass spectrometry (MS) data were acquired in both ESI positive (+) and negative (-) ion modes.

2.6.3. UHPLC-QTOF-MS data processing and statistical analysis

MS data were acquired using Analyst TF 1.81 software (SCIEX). The raw data files in *.wiff.scan format were converted to *.mzML format using ProteoWizard. Subsequent peak processing, including peak alignment, retention time correction, and peak area extraction, was performed using the R programming language[25] (http://cran.r-project.org/). Putative metabolites were identified by comparing MS/MS fragmentation patterns against the HMDB database using a secondary scoring system. For primary MS analysis, a mass error threshold of less than 10 ppm was applied. The processed data were then subjected to partial least squares discriminant analysis (PLS-DA) using the "R" package mixOmics. In addition, differential gene analysis was performed on the Gene Expression Omnibus (GEO) dataset GSE218879 using the R package GEO query[26].

2.6.4. Construction of metabolic pathways and metabolite-gene interaction network

Following normalization, the corresponding compounds of each peak and peak area of each compound were determined. Differentially altered metabolites between each pair of treatment groups were selected based on a variable importance in the projection (VIP) ≥ 1. from PLS-DA. The fold change was calculated the integrated area ratio of the metabolites, while statistical significance was assessed using *p*-values, which were corrected for multiple testing using the Benjamin-Hochberg FDR method. Metabolic pathway analysis was conducted using Metabolite Set Enrichment Analysis (MSEA) within MetaboAnalyst 6.0 (https://www.metaboanalyst.ca/). The KEGG database (http://www.kegg.jp/) was employed to further explore the functional roles and pathway localizations of the identified metabolites. To identify potential molecular links between the observed metabolic changes and gene expression, we cross-referenced the differentially expressed genes with those known to interact with differential metabolites using the Pathway Commons

database (https://www.pathwaycommons.org/). This approach allowed us to identify a set of candidate genes potentially associated with the differentially altered metabolites following gastric mucosal injury. Finally, to visualize the potential interactions between metabolites and genes, we constructed a metabolite-gene interaction network incorporating the overlapping metabolites and their associated genes. Concurrently, we retrieved all genes associated with "gastric mucosal injury" from the GeneCards database[27] (https://www.genecards.org/) and filtered them using the GIFtS score, retaining those above the median to prioritize genes with stronger functional relevance to the disease. We then performed intersection analysis between this high-confidence disease-related gene set and the metabolite-targeted gene set, identifying a core set of overlapping candidates for downstream transcriptional analysis.

2.7 Quantitative real-time PCR

Total RNA was extracted from gastric tissue using Trizol reagent. The concentration of total RNA was determined using a microplate spectrophotometer. cDNA was synthesized from the extracted RNA using a reverse transcriptase kit via reverse transcription. Quantitative real-time PCR (qRT-PCR) was subsequently performed using the KAPA SYBR FAST qPCR kit on the 7300 real-time PCR system (AB Sciex, USA)[25]. The thermal cycling profile consisted of an initial denaturation at 95 ℃ for 2 min, followed by 45 cycles of 95 ℃ for 10 s and 60 ℃ for 31 s. GAPDH was used as the internal control and standard reference gene. All primers for these genes were designed using the NCBI Primer-BLAST tool (http://www.ncbi.nlm.nih.gov/) and synthesized by Tsingke Biotechnology (Nanjing, China), listed in Table S2. Relative gene expression was calculated using the $2^{-\Delta\Delta CT}$ method, comparing treatment groups to the CON group.

2.8 GST pull-down assay and western blot assay

Gastric tissue was homogenized in ice-cold RIPA buffer supplemented with protease and phosphatase inhibitors. Protein concentration was quantified using the BCA Protein Quantification Kit. GST pull-down assays were performed following the manufacturer's protocol using the Active Rac1/Cdc42 Pull-down and Detection Kit.

Protein samples were separated by 12% SDS-PAGE and subsequently transferred to nitrocellulose membranes. After blocking with 5% non-fat milk in TBST for 2 h at room temperature, membranes were incubated overnight at 4 ℃ with primary antibodies, including p-AKT (1:1000), AKT (1:1000), Rac1 (1:1000), Cdc42 (1:1000), and β-catenin (1:1000). Following primary antibody incubation, membranes were treated with horseradish peroxidase (HRP)-conjugated secondary antibodies (anti-rabbit or anti-mouse, 1:5000) for 1 h at room temperature. Protein signals were detected using an enhanced chemiluminescence (ECL) substrate (Biosharp, Shanghai, China) and imaged on a ChemiScope 6100 system (Clinx Science

Instruments, Shanghai, China). Band intensities were quantified by densitometry using Image J (version 1.52a, NIH, USA). β-actin (1:5000) was referenced in this study.

2.9 Nuclear magnetic resonance analysis

For nuclear magnetic resonance (NMR) experiments[28], GBP was depolymerized by 0.1 M TFA at 100 °C for 1 h to lower the viscosity and then neutralized by 0.1 M NaOH to pH 7.0. The hydrolyzate was dissolved into D_2O. All NMR experiments, including ^1H NMR, ^{13}C NMR, correlated spectroscopy (COSY), nuclear overhauser effect spectroscopy (NOESY), heteronuclear single quantum coherence (HSQC), and heteronuclear multiple bond correlation (HMBC) were performed at 25 °C on a Bruker Avance 500 MHz spectrometer (Bruker, Karlsruhe, Germany). Chemical shifts were expressed in parts per million with respect to the 0 ppm point of sodium-3-trimethylsilyl propionate (TSP), used as an internal standard.

2.10 Statistical analysis

Data are presented as means ± standard error of the mean (SEM). Comparisons between two groups were performed using an unpaired Student's t-test. Prior to one-way analysis of variance (ANOVA), normality was assessed using the Shapiro-Wilk test, and variance homogeneity was evaluated using Levene's test. When assumptions were met, a one-way ANOVA was conducted, followed by Tukey's post hoc test for pairwise comparisons. Statistical significance was set at $P < 0.05$, with significance levels denoted as: $^{*}P < 0.05$, $^{**}P < 0.01$, $^{***}P < 0.001$, $^{****}P < 0.0001$ versus the CON group; and $^{\#}P < 0.05$, $^{\#\#}P < 0.01$, $^{\#\#\#}P < 0.001$, $^{\#\#\#\#}P < 0.0001$ versus the MOD group. All statistical analyses were performed using GraphPad Prism 8 software (GraphPad Software, San Diego, CA, USA).

3. Results and discussions

3.1 Ameliorative effects of GEP on gastric mucosal injury in rats

To evaluate the ameliorative effects of GEP against ethanol-induced gastric mucosal injury in rats, macroscopic and histopathological examinations were conducted (Figs. 1 and S1). As shown in Fig. 1B, the CON group exhibited a structurally intact gastric mucosa with a smooth surface and uniform pale erythema, devoid of hemorrhage or edema. Conversely, the MOD group displayed severe mucosal disruption characterized by dark red discoloration and multifocal hemorrhagic patches. Compared with the MOD group, treatment with GEP at 200, and 400 mg/kg (GEP-M and GEP-H) more effectively ameliorated gastric mucosal injury and hemorrhage than the 100 mg/kg dose (GEP-L). Notably, the 200 mg/kg GBP group showed significant therapeutic effects, with nearly no apparent signs of damage in the gastric tissue surface. Histopathological evaluation further that GEP-M, GEP-H, GBP, and OMZ treatments ameliorated the severe structural loss, glandular disorganization, extensive inflammatory infiltration, and edema observed in the

MOD group (Fig. 1C). Remarkably, the GEP-M and GBP groups demonstrated the most significant improvements, maintaining nearly intact mucosal architecture and well-aligned cellular structures, whereas minor bleeding and edema persisted in the GEP-H and OMZ groups. PAS staining (Fig. 1D) revealed that GEP-M and GBP administration significantly restored the depleted mucus secretion and impaired epithelial integrity, which was characterized in the MOD group by enlarged intercellular spaces and weak mucin staining. Quantitatively, the GEP-M and GBP groups at 200 mg/kg significantly attenuated gastric ulcer lesions, with inhibition rates of 82.6% and 78.3%, respectively, which markedly outperformed the GEP-H (66.6%) and GEP-L (30.4%) groups (Fig. 1E). Furthermore, treatment with GEP and GBP led to an increase in gastric pH (Fig. 1F). Consistent with other previous study regarding inflammatory bowel disease[23], GEP the 200 mg/kg exhibited the most pronounced therapeutic efficacy, identifying this concentration as the optimal therapeutic window. Collectively, these findings demonstrate that both the crude GEP-M and the purified GBP exert potent gastroprotective effects, leading to the selection of 200 mg/kg as the optimal dosage for subsequent mechanistic investigations.

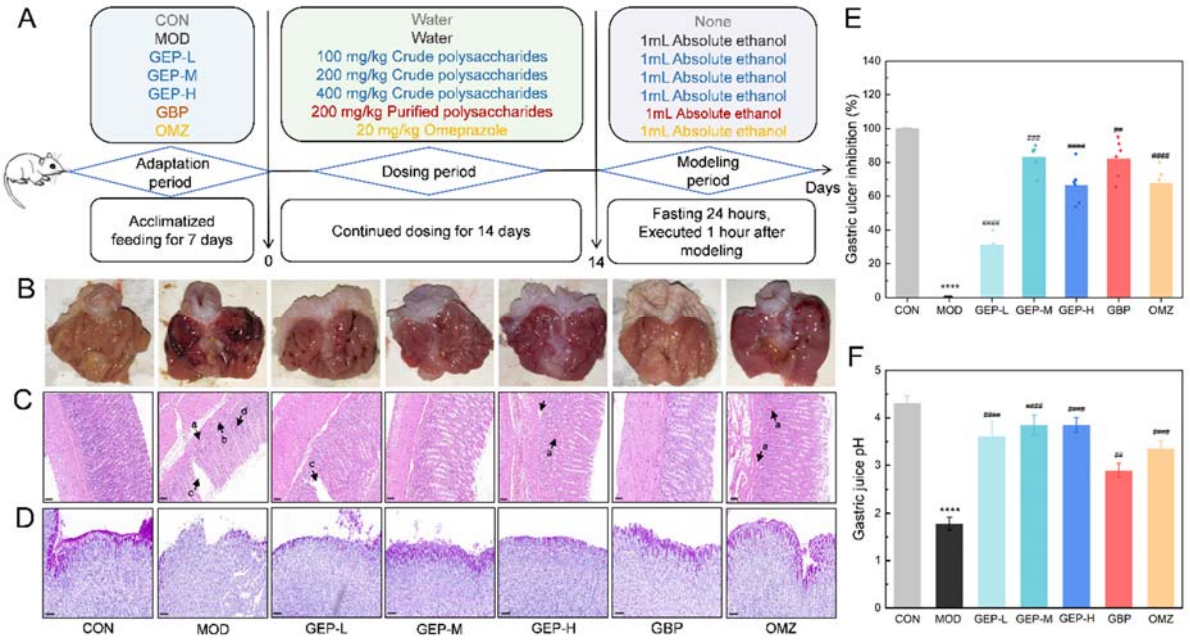

Fig. 1 Experimental design and macroscopic evaluation of the protective effect of GEP. (A) Experimental design of different treatment in rat models against ethanol-induced gastric mucosal injury. (B) Representative macroscopic gastric morphology. (C) Representative HE staining of gastric tissues. The scale bars are 50 μm. Arrows indicate: (a) hemorrhage, (b) submucosal edema, (c) disorganized glandular structure, (d) inflammatory cell infiltration successively. (D) Representative AB-PAS staining of gastric tissues. The scale bars are 100 μm. (E) The gastric ulcer inhibition rate. (F) The pH value of gastric juice.

3.2 Effects of GEP on oxidative stress and inflammatory response

Oxidative stress plays key role in the pathogenesis of gastric mucosal injury through multiple mechanisms. To evaluate the antioxidant potential of GEP, we quantified key biomarkers-including SOD, GSH, NO and MDA. Under the stimulation of ethanol, the activity of SOD is inhibited, and GSH and NO are substantially reduced (Figs. 2A-C). The inhibition of SOD impaired the clearance of superoxide anion radicals

($O_2^{\bullet-}$), resulting in the accumulation of this primary reactive oxygen species (ROS)[29,30]. NO was rapidly consumed through its reaction with $O_2^{\bullet-}$, leading to the formation of peroxynitrite ($ONOO^-$), a potent reactive nitrogen species (RNS). The depletion of GSH further compromised the cellular capacity to detoxify $ONOO^-$, collectively exacerbating the accumulation of RNS. The accumulated ROS and RNS trigger lipid peroxidation (LPO), which damages cell membrane phospholipids and generates the cytotoxic byproduct MDA in the MOD group (Fig. 2D), thereby exacerbating oxidative damage to cells. In contrast, treatment with GEP-M and GBP significantly enhanced the activity of SOD, elevated the levels of GSH, and decreased the levels of MDA. SOD catalyzes superoxide anions into hydrogen peroxide, while GSH neutralizes the hydrogen peroxide, thereby maintaining redox balance and alleviating oxidative stress[31,32]. Furthermore, GEP-M and GBP treatments restored NO concentrations to a normal physiological level (1 μmol/gprot), comparable to the CON group (Fig. 2C). At this level, NO contributes to the gastric mucosal protection by regulating mucosal blood flow and mucus secretion[33]. Taken together, these results demonstrate that GEP alleviate oxidative damage by reducing the accumulation of ROS, RNS and LPO-derived products, thereby protecting cells from damage.

In the acute gastric mucosal injury model, changes in PGE_2 and EGF levels are closely associated with the severity of gastric mucosal damage. Under conditions of severe oxidative stress, the production of PGE_2 and EGF is reduced in the MOD group (Figs. 2E-F). However, administration of GEP-M and GEP-H led to a marked increase in the levels of PGE_2 and EGF in the gastric mucosa. PGE_2 stimulates gastric mucosal cells to secrete bicarbonate, which helps neutralize gastric acid and reduce acidity. Meanwhile, EGF inhibits gastric acid secretion, further lowering the acid level[34]. Consistent with our findings, treatment with GEP and GBP significantly increased gastric pH (Fig. 1F), indicating a reduction in gastric acidity. In addition, PGE_2 promotes the secretion of mucus, forming a protective barrier that prevents direct erosion of the gastric mucosa[35]. In the GEP-M group, a significant increase in the immunofluorescence intensity of EGF protein was observed (Figs. 2G-H), indicating a significant upregulation of EGF expression in the gastric tissue. EGF is capable of stimulating the proliferation and differentiation of gastric mucosal epithelial cells[36], thereby facilitating the protection and repair of gastric mucosal injury. During the treatment process, the restoration of EGF levels can serve as an important indicator for evaluating the therapeutic efficacy. Research has also found that the levels of EGF in the gastric juice of patients with chronic gastritis are significantly lower than those in healthy individuals[37]. This suggests that a decrease in EGF levels may be associated with the inflammatory response of the gastric mucosa.

Ethanol induces the inflammatory response in gastric mucosal cells[38], leading to the excessive release of proinflammatory cytokines such as *IL-1β*, *IL-6*, and *TNF-α*, thereby triggering an acute inflammatory response in the gastric mucosa[39]. Therefore, the levels of these cytokines were evaluated in gastric tissue (Figs. 2I-K). Gastric mucosal injury significantly upregulated the mRNA expression of *IL-1β*, *TNF-α* and *IL-6* in gastric tissue compared with the CON group. Moreover, proinflammatory cytokines can induce the overproduction of ROS in gastric mucosal cells[40,41]. These ROS can damage cell membranes, proteins, and DNA, leading to cellular dysfunction and death[42]. However, administration with GEP-M, GEP-H and GBP significantly downregulated the mRNA expression of these cytokines. These results indicate that the administration of GEP exerts the anti-inflammatory effect, which may underlie its therapeutic potential in treating gastric mucosal injury.

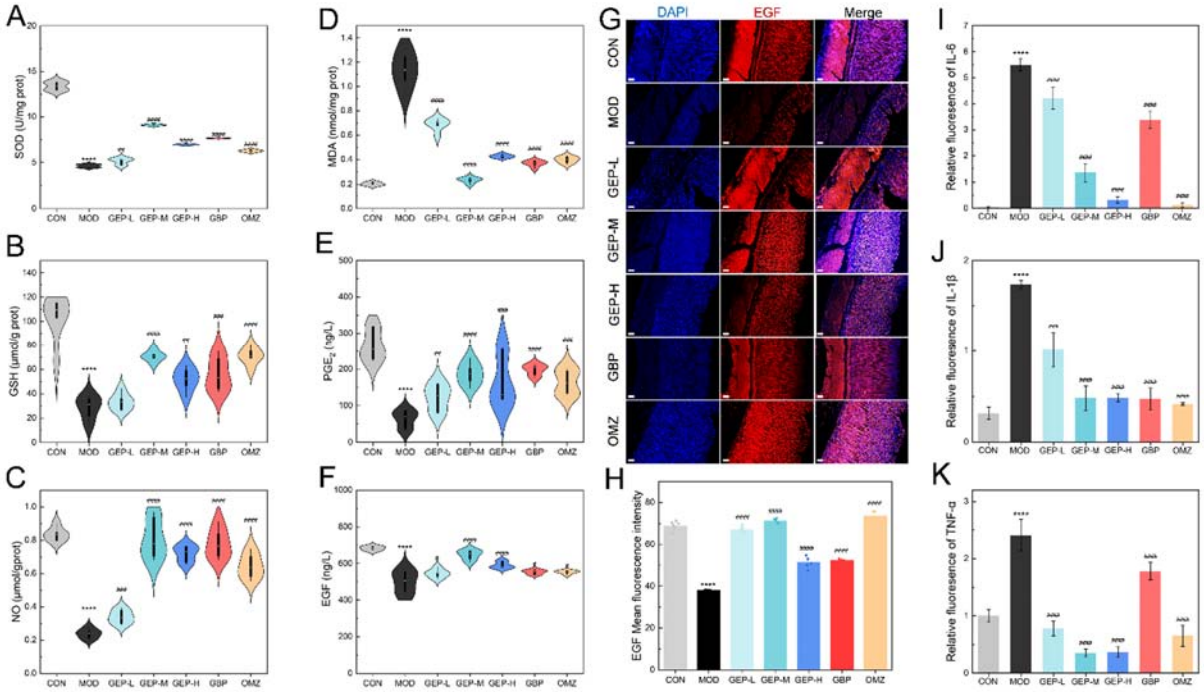

Fig. 2 Effects of GEP on oxidative stress and inflammatory response. The activity of SOD (A), GSH (B), NO (C) and MDA (D) in gastric tissue. The levels of PGE_2 (E) and EGF (F) in gastric tissue. (G) The immunofluorescence images of EGF. The scale bars are 50 μm. (H) Quantification of the immunofluorescence intensity of EGF. The mRNA expression of *IL-6* (I), *IL-1β* (J) and *TNF-α* (K) in gastric tissue.

3.3 Effects of GEP on gastrointestinal microbiota

3.3.1 Effects of GEP on gastrointestinal microbiota at the phylum level

The dysbiosis of the gut microbiota plays a significant role in the pathogenesis of gastric mucosal injury, gastritis, and gastric cancer[9]. To elucidate the effects of GEP on the microbiota, we performed 16S rRNA gene sequencing to assess the alterations in the composition of both gastric and intestinal microbiota following administration of GEP. The species richness and diversity of microbiota in the gastric contents and fecal samples were analyzed by calculating alpha diversity indices, including OS, Shannon index, and Pielou_evenness indices (Figs. 3A-B, Fig. S2). Gastric mucosal injury in rats resulted in a significant

reduction in the OS and Shannon index in gastric contents, indicating that the richness and evenness of the gastric microbial community were severely disrupted. These changes are likely related to the local microenvironmental disturbances caused by ethanol-induced gastric mucosal injury, such as changes in increased oxidative stress, gastric pH, and the release of inflammatory cytokines. Compared with the MOD group, the GEP-M and GBP groups significantly increased the OS in the gastric microbiota, leading to a more balanced gastric community structure. In contrast, although the OS and Shannon index of the fecal microbiota exhibited a decline, this reduction did not attain statistical significance (Fig. 3B, Fig. S2B). This may be because the fecal microbiota primarily reflects the overall state of the gut microbiota, while gastric mucosal injury directly affects the gastric microenvironment. The stomach and intestine are separated by certain physiological barriers, and changes in the gastric microenvironment may not immediately or significantly impact the composition and function of the intestinal microbiota[43]. However, alterations in the gastric microenvironment can indirectly influence the intestinal microbiota through mechanisms such as the transfer of metabolites and immune modulation. Notably, treatment with GEP-M significantly enhanced the Shannon index of the intestinal microbiota (Fig. S2B). Additionally, the Pielou_evenness index of the GEP-M group was closer to 1, indicating higher diversity in gastrointestinal microbiota (Figs. S2C-D). Thus, the administration of GEP enhanced the richness and diversity of both gastric and intestinal microbiota.

At the phylum level, Bacillota is identified as one of the predominant phyla within the gastric and intestinal microbiota of rats (Figs. 3C and D). The dominant phyla in the rat stomach included Pseudomonadota, Bacteroidota, and Actinomycetota, while those in the intestine are Bacteroidota, Pseudomonadota, and Actinobacteriota. Acid-resistant bacteria dominate the gastric mucosa[44], with *H. pylori* being the most clinically relevant representative, belonging to the Pseudomonadota phylum[45]. Following ethanol-induced gastric mucosal injury, the relative abundance of Pseudomonadota in the gastric microbiota of the MOD group increased, whereas that of Bacillota decreased (Fig. 3C). Concurrently, the relative abundance of Bacteroidota in the intestinal microbiota of the MOD group decreased (Fig. 3D). Administration of GBP reduced the abundance of Pseudomonadota and increased that of Bacillota in the gastric microbiota. Moreover, both GBP and GEP-M administration led to an increase in the relative abundance of Bacteroidota in the intestinal microbiota.

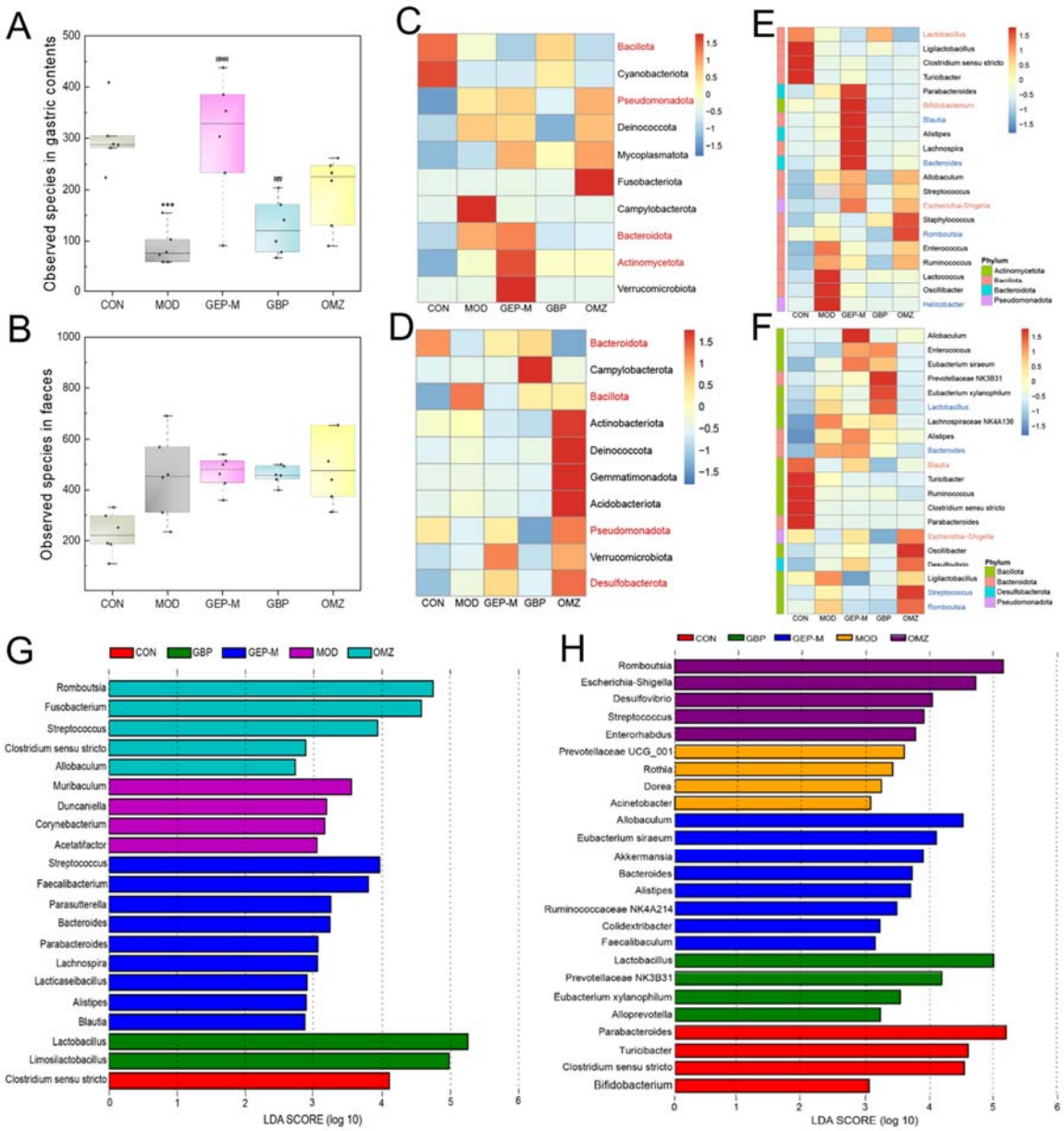

Fig. 3 Effects of GEP on gastrointestinal microbiota. The observed species in gastric content (A) and (B). The relative abundance of gastric microbiota (C) and intestinal microbiota (D) at the phylum level. The relative abundance of gastric microbiota (E) and intestinal microbiota (F) at the genus level. Red indicates increased abundance following GEP treatment, while blue indicates decreased abundance. Enrichment of certain taxa with an LDA score higher than 2 in gastric content (G) and faeces (H).

3.3.2 Effects of GEP on gastrointestinal microbiota at the genus level

Ethanol-induced gastric mucosal injury resulted in a significant increase in the abundance of the genus *Helicobacter* within the phylum Pseudomonadota in the stomach (Fig. 3E, Table S3). *H. pylori* is the most prevalent pathogenic microorganism in the stomach and is strongly linked to the development of gastritis, gastric ulcers and gastric cancer[46,47]. However, treatment with GBP and GEP-M effectively mitigated this increase in *Helicobacter* abundance, potentially preventing its progression to more severe gastric diseases. At the genus level, GBP administration also decreased the relative abundance of *Escherichia-Shigella* within the phylum Pseudomonadota and *Bacteroides* within the phylum Bacteroidota. As pathogenic microorganisms

within the phylum Pseudomonadota, *Escherichia-Shigella* and *Helicobacter* trigger robust immune responses, including the recruitment of inflammatory cells and the release of inflammatory cytokines *TNF-α*, *IL-6* and *IL-1β*[5,48], leading to inflammation and damage of the gastrointestinal mucosa. Moreover, they can disrupt the gastric microbiota balance by suppressing the growth of beneficial bacterial communities. Conversely, GBP administration increased the relative abundance of the probiotic genus *Lactobacillus*. GEP-M administration, on the other hand, increased the relative abundance of the probiotic genus *Bifidobacterium* and the potential probiotic genus *Blautia*. Studies have indicated that *Lactobacillus* can competitively inhibit the growth of *H. pylori*[49], thereby reducing the inflammatory response it induces. *Blautia* has been reported to prevent pathogen colonization by producing bacteriocins and to exhibit anti-inflammatory properties by modulating T cells[50]. A deficiency in *Bifidobacterium* may indirectly promote the development of gastric cancer[51]. These probiotics protect the gastric mucosa by maintaining the balance of the gastric microbiota, inhibiting the growth of harmful bacteria, and modulating immune responses.

In fecal samples, *Helicobacter* was not detected (Fig. 3F, Table S4), highlighting the importance of distinguishing between gastric mucosa-associated and fecal microbiota when studying gastric diseases. The relative abundance of *Escherichia-Shigella* was also decreased in the intestinal microbiota following GBP administration. This indicates that *Escherichia-Shigella* in gastric mucosal injury involve in both gastric and intestinal dysbiosis. Notably, the relative abundance of *Streptococcus* within the phylum Bacillota was increased in the MOD group (Fig. 3F). In patients with gastritis, the abundance of *Streptococcus* may increase due to reduced gastric acid secretion[52]. Additionally, *Streptococcus* is significantly enriched in the oral cavity, stomach, and intestines of patients with gastric cancer[12]. Both GBP and GEP-M treatments reduced the relative abundance of *Streptococcus*. GBP administration also decreased the relative abundance of *Bacteroides*, thus exerting a protective effect on the gastric mucosa. Consistent with the changes observed in the gastric microbiota, GBP administration increased the relative abundance of *Lactobacillus*, while GEP-M administration increased that of *Blautia*. Although there are limited studies directly linking *Blautia* to gastritis. Existing research suggests that *Blautia* can modulate the intestinal immune response and reduce inflammation by producing short-chain fatty acids such as butyrate[50]. Its specific mechanisms of action in gastritis and gastric cancer still require further investigation. It is worth noting that *Lactobacillus* emerged as the dominant genus in both the gastric and intestinal microbiota of the GBP group (Figs. 3G-H). In contrast, *Streptococcus* was the dominant genus in the gastrointestinal microbiota of the OMZ group. Therefore, the therapeutic effects of GEP are likely mediated through increasing the abundance of probiotics (such as *Lactobacillus* and *Bifidobacterium*) while reducing the abundance of pathogenic bacteria (such as *Helicobacter*,

Escherichia-Shigella, and *Streptococcus*). This effectively restores the balance of the gastrointestinal microbiota, thereby exerting a potentially positive role in the prevention and treatment of gastric mucosal injury.

3.4 Effects of GEP on the gastrointestinal metabolic profile in gastric mucosal injury

Gastrointestinal metabolism is intricately connected to gastric mucosal injury[53]. Metabolic processes impact gastric mucosal health and are crucial for the development, progression, and repair of gastric mucosal injury[54]. To explore this, we used metabolomics to analyze changes in gastric metabolites and elucidate the metabolic mechanisms underlying the protective effects of GEP on gastric mucosal injury. PLS-DA score plots (Figs. 4A-B) showed that the GBP and GEP-H groups were situated between the MOD and CON groups, whereas the GEP-M and GEP-L groups were clearly segregated from the MOD and CON groups. Based on the therapeutic and gastrointestinal microbiota analysis results, we focused particularly on the metabolic differences between the GBP and GEP-M groups compared to the MOD and CON groups. A total of 61 significantly different metabolites were identified among the GBP, GEP-M, CON, and MOD groups (Fig. 4C). As depicted in Figs. 4D-E and Table S5, pathway enrichment analysis revealed that these metabolites were significantly enriched in several key metabolic pathways, including the tricarboxylic acid (TCA) cycle, alanine, aspartate and glutamate metabolism, pyruvate metabolism, tryptophan metabolism, glycolysis, primary bile acid biosynthesis, steroid hormone biosynthesis, and other pathways. Gastric mucosal injury induced by ethanol triggers oxidative stress and inflammatory responses, which in turn affect the function of cellular mitochondria, prompting cells to shift towards glycolysis[22]. This metabolic switch leads to the accumulation of pyruvate and lactate, along with the consumption of phosphoenolpyruvate (Fig. 4C). The administration of GEP-M and GBP effectively improved cellular energy metabolism, resulting in reduced lactate levels and decreased dependence on glycolysis, thereby improving the intracellular acidic environment. Furthermore, GBP restored the metabolic function of TCA cycle caused by gastric mucosal injury and regulated the levels of related metabolites such as α-ketoglutarate, citrate, oxaloacetate, fumarate, and succinate (Fig. 4E).

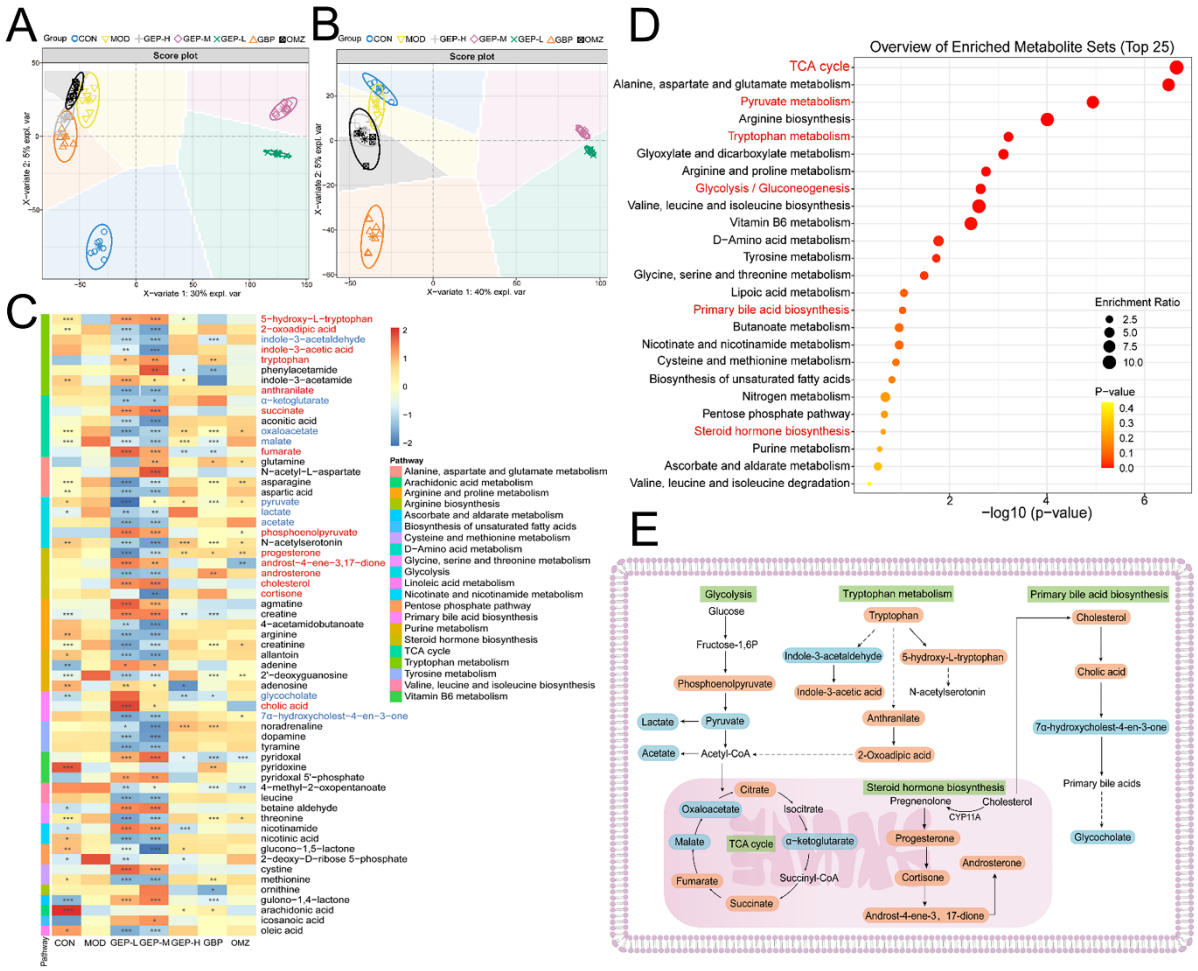

Fig. 4 Effects of GEP on the gastrointestinal metabolic profile. PLS-DA score plots of gastric metabolites in negative (A) and positive (B) ionization modes. (C) Heatmap of significantly different metabolites among the seven groups. (D) Overview of the top 25 enriched metabolic pathways. (E) Significant altered metabolic profiles after treatment with GBP. Red indicates metabolites with significantly increased levels following GBP treatment, whereas blue indicates metabolites with significantly decreased levels.

Gastric mucosal injury is typically accompanied by inflammatory, which significantly activate tryptophan metabolism[55]. In this study, gastric mucosal injury led to alterations in tryptophan metabolism, characterized by decreased levels of tryptophan and 5-hydroxy-L-tryptophan (Fig. 4C). This aligns with findings showing reduced tryptophan levels in various chronic inflammatory diseases[56]. However, treatment with GEP-M and GBP significantly increased the levels of tryptophan and 5-hydroxy-L-tryptophan, which is likely to promote the repair of the gastric mucosa. Notably, the GBP group exhibited a significant elevation in the level of indole-3-acetic acid. Indole metabolites, such as indole-3-acetic acid (IAA), produced by gut microbiota, can enhance mucosal barrier function by activating the aryl hydrocarbon receptor (AhR)[43]. Activation of AhR can modulate the production of anti- and pro-inflammatory cytokines, which help in reducing inflammation[57]. Therefore, the changes in tryptophan metabolism induced by GEP can impact the protection of the gastric mucosa. Moreover, GEP also regulated the metabolic disorders of steroid hormone biosynthesis and primary bile acid biosynthesis induced by

ethanol. Progesterone and cortisone have been reported to inhibit the NF-κB pathway via their receptors[58], thereby reducing the release of pro-inflammatory cytokines. In this study, the GBP group exhibited increased levels of progesterone and cortisone, which is consistent with the observed decrease in *IL-6* and *TNF-α* levels. This suggests that these hormones may help alleviate inflammation-induced damage to the gastric mucosa. Additionally, progesterone can also promote mucus secretion and epithelial cell proliferation, thereby enhancing the protective function of the gastric mucosa. Abnormalities in primary bile acid biosynthesis can trigger inflammatory responses, exacerbating gastric mucosa injury. Therefore, GEP appear to restore the inflammation-induced imbalance in gastric homeostasis by regulating the metabolic pathways such as TCA cycle, glycolysis, tryptophan metabolism, steroid hormone biosynthesis, and primary bile acid biosynthesis.

To investigate the correlation between altered gastric microbiota at the genus level and gastric metabolites, Spearman's correlation analysis was employed (Fig. 5). The analysis revealed that levels of *Bifidobacterium* and *Blautia* were positively correlated with tryptophan and 5-hydroxy-L-tryptophan levels. Meanwhile, *Lactobacillus* abundance showed a positive correlation with IAA levels. Notably, certain *Lactobacillus* strains, such as *Lactobacillus reuteri*, have been identified for their ability to produce IAA through tryptophan metabolism[59]. This metabolic activity of *Lactobacillus* may contribute to reducing inflammation via the production of IAA. Conversely, the abundances of *Escherichia-Shigella* and *Bacteroides* were negatively correlated with IAA levels. These findings suggest that IAA production has significant implications for gastric health and immune regulation. Regarding steroid hormone biosynthesis, *Lactobacillus* abundance was positively correlated with cortisone levels, whereas *Escherichia-Shigella* and *Bacteroides* abundance were negatively correlated with cortisone and progesterone levels. Our results indicate a strong correlation between shifts in probiotics and pathogenic bacteria populations, and changes in metabolites involved in tryptophan metabolism and steroid hormone biosynthesis. This correlation analysis provides insights into the functional relationship between the altered gastric microbiota and dysregulated gastric metabolites, which may help elucidate the mechanisms by which GEP exert their effects on gastric mucosal injury.

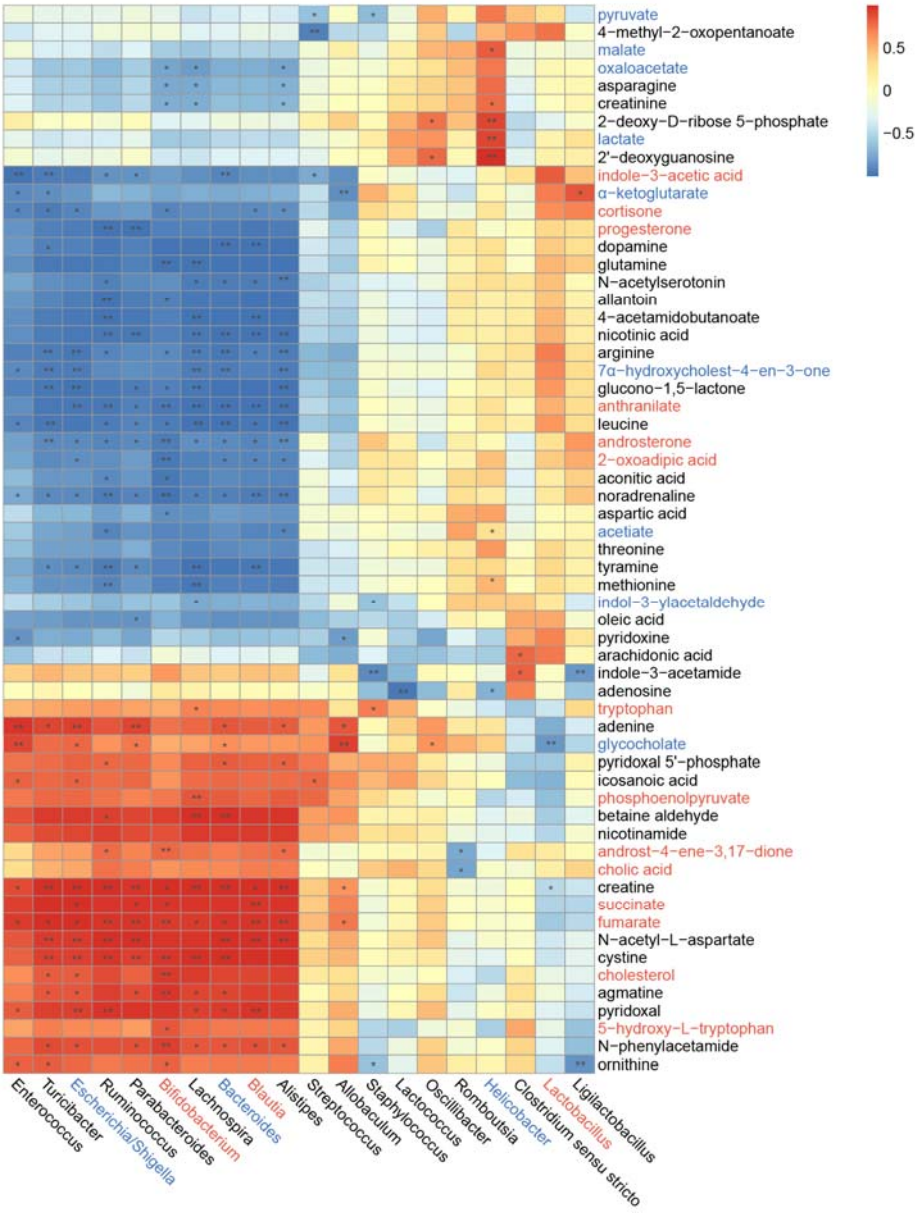

Fig. 5 Heatmap visualizing Spearman's correlations between gastric microbiota at the genus level and altered metabolites.

3.5 Transcriptional modulation of GEP in gastric mucosal injury through metabolite-gene interaction network

By employing bioinformatics analysis to identify the upstream genes interacting with the differentially enriched metabolites, we constructed a visual network depicting metabolite-gene interactions (Fig. 6A). This comprehensive analysis uncovered 94 key genes directly linked to these differential metabolites, presenting potential targets for further investigation into the molecular mechanisms underlying the effects of GEP in ameliorating gastric mucosal injury. As illustrated in Fig. 6B, 1977 genes highly associated with gastric mucosal injury were identified from the human gene database GeneCards. Further, intersection analysis between this gene set and the 94 metabolite-targeted genes from our network model revealed a core set of 31 overlapping genes. These 31 candidates were subsequently subjected to transcriptional analysis to evaluate their expression patterns and potential functional roles in gastric mucosal injury. Ultimately, 10 significantly

altered genes were identified (Figs. 6C and D), primarily involved in the Calcineurin/NFATc1 and PI3K/Rac1 signaling pathways (Fig. 6E). Treatment with ethanol leads to congestion and edema in the gastric mucosa, followed by tissue necrosis. Following gastric mucosal injury, increased membrane permeability causes the opening of calcium channels, leading to an influx of calcium ions and subsequent activation of calcineurin[60]. Activated calcineurin dephosphorylates NFAT, allowing its translocation into the nucleus, where it initiates gene transcription and triggers inflammatory process[61]. Consistent with our findings, the mRNA expression level of *Nfatc1* was significantly increased in the MOD group (Fig. 6C). However, treatment with GEP significantly reduced *Nfatc1*expression in a dose-dependent manner, thereby suppressing inflammation. *Nfatc1* can directly bind to the promoter region of the *Notch3* and *Sox2* genes, and its expression affects the expression of *Notch3* and *Sox2*[61]. Activation of *Notch3* can promote the proliferation of vascular smooth muscle cells, which is a key step in the process of vascular remodeling and new blood vessel formation. The GEP-H group and GBP group, as well as the OMZ group, significantly activated the expression of *Notch3*. These results suggest that GEP may promote cell proliferation and vascular remodeling by modulating the Calcineurin/NFATc1 signaling pathway.

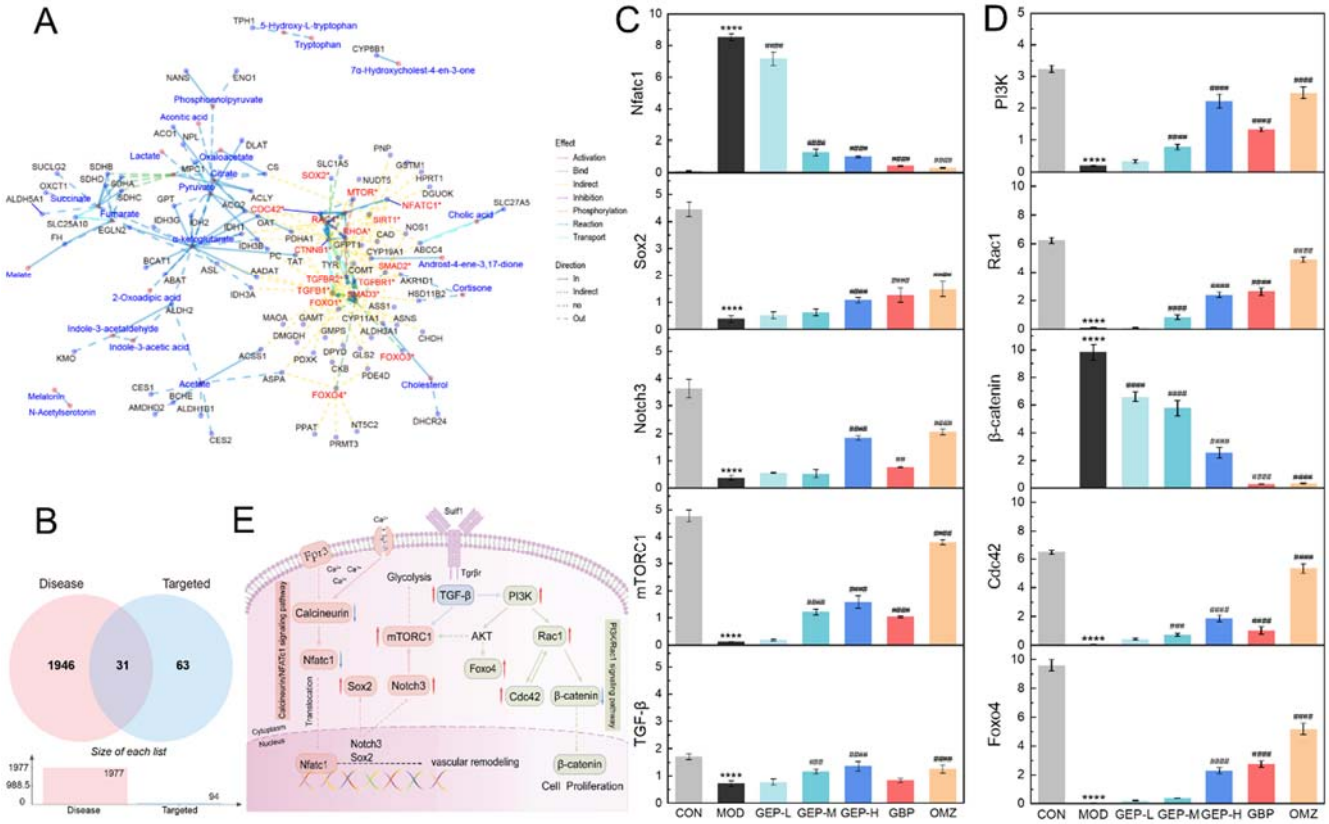

Fig. 6 Transcriptional modulation of GEP in gastric mucosal injury. (A) Metabolite-gene interaction network. (B) Venn plot and bar chart of showing the overlap between metabolite-targeted genes and gastric mucosal injury-related genes. The pink set represents genes associated with gastric mucosal injury; the blue set indicates metabolite-targeted genes after treatment with GEP. (C) mRNA expression levels of *Nfatc1*, *Sox2*, *Notch3*, *mTORC1* and *TGF-β* in gastric tissue. (D) mRNA expression levels of *PI3K*, *Rac1*, *β-catenin*, *Cdc42* and *Foxo4* in gastric tissue. (E) Significantly altered signaling pathways correlated with key metabolites after treatment with GBP. Red arrows indicate upregulation, blue arrows indicate downregulation.

TGF-β, *Rac1*, *Cdc42*, and *β-catenin* are pivotal signaling molecules that regulate cell proliferation and apoptosis, essential for maintaining gastric mucosa homeostasis[62–64]. Compared with the CON group, ethanol-induced gastric mucosal injury significantly reduced the mRNA expression levels of *TGF-β*, *Rac1*, and *Cdc42*, while significantly increasing the mRNA expression level of *β-catenin*. As a multifunctional cytokine, *TGF-β* suppresses inflammatory cytokine production and activates the PI3K/AKT signaling pathway via *Smad3* -dependent mechanism in vascular smooth muscle cells[62,65], thereby promoting cell proliferation and tissue repair. In this study, the mRNA expression level of *TGF-β* was significantly elevated in the GEP-H and GEP-M groups (Fig. 6C), with the observed reduction in inflammatory cytokines shown in Figs. 2I-K and further indicating activation of the PI3K/AKT signaling pathway (Fig. 6D). Yan et al. discovered that cinnamaldehyde significantly ameliorates gastric mucosal injury by activating the PI3K/Akt signaling pathway, which regulates gastric epithelial cell apoptosis while mitigating inflammation and oxidative stress[65]. The activation of this cascade is initiated by the PI3K-catalyzed production of phosphatidylinositol-3,4,5-trisphosphate (PIP3). As a critical second messenger, PIP3 recruits and phosphorylates various downstream effectors, including Akt, Rac1, and Cdc42. Previous research has demonstrated that treatment of gastric cancer cells with the Rac1-specific inhibitor leads to a marked reduction in their migratory and invasive capacities, suggesting that Rac1 is a pivotal factor mediating cellular mobility and regeneration during the process of gastric mucosal repair[66]. Rac1 and Cdc42, members of the Rho GTPase family, are crucial regulators of epithelial cell migration, proliferation, and apoptosis[63]. In their GDP-bound state, these proteins remain inactive, which impairs the formation of cellular protrusions, thereby inhibiting the migration of gastric mucosal epithelial cells to the injury site and exacerbating mucosal damage. However, activated Rac1 not only promotes cytoskeletal reorganization and cell migration but also stabilizes the E-cadherin/β-catenin complex, thereby reinforcing intercellular adherens junctions[67,68] and supporting the integrity of the gastric mucosal barrier. Our results demonstrate that, compared with the MOD group, treatment with GEP—except in the GEP-L group—significantly upregulated the mRNA expression levels of *Rac1* and *Cdc42* while effectively suppressing the aberrant overexpression of *β-catenin*. These findings suggest that GEP may ameliorate ethanol-induced gastric mucosal injury by activating the PI3K/Rac1 signaling pathway.

3.6 GEP alleviate gastric mucosal injury by activating the PI3K/Rac1 signaling pathway

This regulatory cascade, extending from metabolic shifts to the activation of the PI3K/Rac1 signaling axis, was identified using a metabolite–gene interaction network as a functional molecular bridge. To experimentally validate the mechanism by which GEP modulates this pathway, we quantified the expression

and activation levels of its core components within gastric mucosal tissues. Specifically, the activation status of Rac1 and Cdc42 was assessed using GST pull-down assays, allowing for the selective isolation of their GTP-bound isoforms (Rac1-GTP and Cdc42-GTP). These active forms, alongside key upstream transducers and downstream effectors, were further characterized via Western blot analysis to provide a comprehensive map of the signaling response induced by GEP (Figs. 7 and S3). The results revealed that changes at the protein level (Figs. 7A and B) were highly consistent with those observed at the transcriptional level. Compared with the CON group, the MOD group exhibited significantly reduced protein levels of p-AKT, Rac1-GTP, and Cdc42-GTP, indicating suppression of the PI3K/Rac1 signaling pathway and reduced activity of its downstream effectors, Rac1 and Cdc42. In contrast, β-catenin protein expression was markedly elevated in the MOD group, reflecting its pathological cytoplasmic accumulation. Notably, treatment with GEP—particularly in the GEP-M and GBP groups—significantly restored the expression levels of p-AKT, Rac1-GTP, and Cdc42-GTP, while effectively suppressing the aberrant overexpression of β-catenin (Fig. 7C). These findings strongly suggest that GEP activates the PI3K/Rac1 signaling pathway, thereby promoting the GTP-bound (i.e., active) state of Rac1 and Cdc42. Previous studies have demonstrated that activated Rac1 drives the formation of lamellipodia in gastric epithelial cells, facilitating cell migration and accelerating the repair of injured mucosa. Meanwhile, activated Cdc42 primarily promotes cell proliferation by regulating cell cycle progression, specifically by enhancing the G1-to-S phase transition[69]. Moreover, activated Rac1 can induce the translocation of β-catenin from the cytoplasm to the nucleus, where it forms a complex with TCF/LEF transcription factors to initiate the transcription of downstream proliferation-related genes, thereby further enhancing tissue regeneration[70]. Thus, both activated Rac1 and Cdc42 play pivotal roles in maintaining the integrity of the gastric epithelial barrier. In summary, GEP exerted protective effects against ethanol-induced gastric mucosal injury by activating the PI3K/Rac1 signaling axis, effectively restoring Rac1 and Cdc42 activity, and promoting gastric epithelial cell migration and proliferation—ultimately contributing to the restoration of mucosal homeostasis.

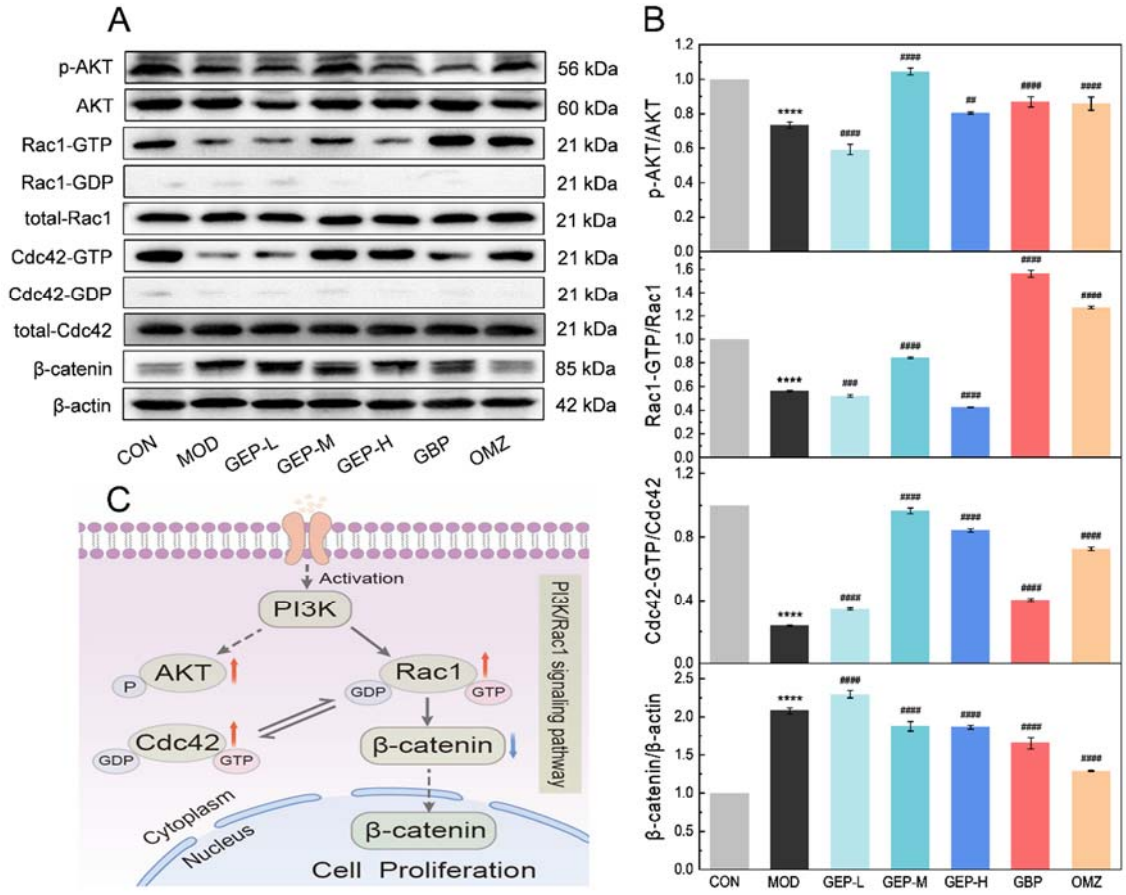

Fig. 7 GEP alleviate gastric mucosal injury by activating the PI3K/Rac1 signaling pathway (A) Representative Western blot images of p-AKT, AKT, Rac1-GTP, Rac1-GDP, total-Rac1, Cdc42-GTP, Cdc42-GDP, total-Cdc42 and β-catenin. (B) Quantitative analysis of relative protein expression levels. (C) Schematic diagram illustrating significant changes in key proteins of the PI3K/Rac1 signaling pathway. Red arrows indicate upregulation, blue arrows indicate downregulation.

3.7 The chemical composition and structural characteristics of GBP

In our previous study[23], a fundamental structural characterization of purified GBP were achieved by determining its monosaccharide composition (Table S6), molar mass, and molecular radius (Table S7). GBP is predominantly composed of glucose (98.03%), along with galactose, rhamnose, arabinose, and glucuronic acid. Molecular weight analysis revealed that GBP possesses a weight-average molecular weight (Mw) of 1.435×10^6 g/mol and a number-average molecular weight (Mn) of 2.279×10^5 g/mol. In this study, the fine structural characteristics of GBP were further elucidated through methylation analysis (Table 1) and NMR spectroscopy (Table 2, Fig. 8), allowing for a detailed determination of its glycosidic linkages and repeating units. As summarized in Table 1, methylation analysis was carried out to determine the glycosyl linkage pattern. It indicated that there were five partially methylated alditol acetates (PMAAs) identified as 1,5-di-O-acetyl-2,3,4,6-tetra-O-methyl glucitol,1,4,5-tri-O-acetyl-2,3,6-tri-O-methyl glucitol,1,3,4,5-tetra-O-acetyl-2,6-di-O-methyl glucitol,1,2,4,5-tetra-O-acetyl-3,6-di-O-methyl glucitol, and 1,4,5,6-tetra-O-acetyl-2,3-di-O-methyl glucitol based on GC-MS databases and relevant literature[71,72]. GBP is composed of t-Glcp, 4-Glcp, 3,4-Glcp, 2,4-Glcp, and 4,6-Glcp in a molar ratio of 7.36:83.30:1.90:1.21:6.23.

Subsequent NMR analysis was used to further determine the structural linkages (Fig. 8). As shown in Figs. 8A and B, the hydrogen spectrum signals of GBP are mainly concentrated in the range of δ3.2-5.7 ppm, and the carbon spectrum signals are mainly concentrated in the range of δ60-106 ppm, indicating that it has the characteristic absorption peaks of polysaccharides. By combining the cross-peaks in the anomeric region of the ^{13}C NMR spectrum and the HSQC spectrum, the anomeric signals present in GBP were identified as: δ5.41/102.51, δ4.98/101.42, δ5.4/102.39, δ5.41/102.37, and δ5.26/103.67, which were respectively designated as sugar residues A, B, Ca, Cb, and Cc (Fig. 8). Due to the significant spectral overlap arising from the highly similar chemical shifts of →4)-α-D-GalAp-(1→ (Signal A) and other glucosyl linkages (Signal C, including →2,4)-α-D-Glcp-(1→, →3,4)-α-D-Glcp-(1→ and →4,6)-α-D-Glcp-(1→, these residues could not be independently resolved in the NMR spectra. Quantitative integration of the ^{1}H and ^{13}C NMR spectra yielded combined proportions (A+C) of 96.33% and 90.33% (Tables S8 and S9), respectively, which are in close agreement with the corresponding ratio of 92.64% derived from the methylation analysis. Further in-depth analysis using various two-dimensional NMR spectra led to the assignment of the carbon and hydrogen chemical shifts for each sugar residue, as shown in Table 2. All the above data indicated GBP is composed of a backbone structure linked by →4)-α-D-Glcp-(1→ units. The side chains are mainly constituted by →2,4)-α-D-Glcp-(1→, →3,4)-α-D-Glcp-(1→ and →4,6)-α-D-Glcp-(1→units (Fig. S4).

Table 1 Methylation analysis of GBP

Glycosidic linkage	Derivative name	M_W	Relative molar ratio (%)
t-Glc(p)	1,5-di-O-acetyl-2,3,4,6-tetra-O-methyl glucitol	323	7.36
4-Glc(p)	1,4,5-tri-O-acetyl-2,3,6-tri-O-methyl glucitol	351	83.30
3,4-Glc(p)	1,3,4,5-tetra-O-acetyl-2,6-di-O-methyl glucitol	379	1.90
2,4-Glc(p)	1,2,4,5-tetra-O-acetyl-3,6-di-O-methyl glucitol	379	1.21
4,6-Glc(p)	1,4,5,6-tetra-O-acetyl-2,3-di-O-methyl glucitol	379	6.23

Table 2 The ^{1}H NMR and ^{13}C NMR shifts (ppm) of GBP

Code	Glycosyl residues	Chemical shifts(ppm)					
		H1/C1	H2/C2	H3/C3	H4/C4	H5/C5	H6/C6
A	→4)-α-D-Glcp-(1→	5.41	3.65	3.97	3.67	3.83	3.86,3.63
		102.51	74.29	76.09	79.53	73.92	63.18
B	α-D-Glcp-(1→	4.98	3.61	3.71	3.44	3.76	3.86,3.66
		101.42	75.46	75.63	75.16	73.93	63.18
Ca	→4,6)-α-D-Glcp-(1→	5.4	3.63	3.86	3.98	3.67	3.85,3.44
		102.39	74.49	73.93	79.64	74.29	72.07
Cb	→2,4)-α-D-Glcp-(1→	5.41	3.53	3.83	3.98	3.88	3.9-3.97
		102.37	79.47	75.77	80.47	74.67	64.67
Cc	→3,4)-α-D-Glcp-(1→	5.26	3.77	4	3.85	3.85	3.69-3.72
		103.67	74.27	81.57	80.97	74.67	64.67

The structural characterization of GBP exhibits a significant resemblance to PGE, a homogeneous polysaccharide isolated from *Gastrodia elata* by Zhu et al.[73], which similarly features a →4)-α-D-Glcp-(1→

backbone with →4,6)-α-D-Glcp-(1→ and →3)-α-D-Glcp-(1→ linked side chains and a molecular weight (1.54×10^3 kDa) comparable to that of GBP. From a physicochemical perspective, the relatively low Mw and high branching degree of such α-glucans increases the frequency of effective collisions between polysaccharide molecules and free radicals, thereby facilitating superior antioxidant activity[74,75]. Furthermore, (1→4)-linked Glcp polysaccharides have been reported to enhance cell membrane integrity, suppress oxidative stress, and promote the repair of cellular damage[15,76]. The fundamental mechanism underlying these protective effects is attributed to the abundance of accessible hydroxyl groups, which serve as efficient hydrogen donors to neutralize free radicals. Notably, the gastroprotective polysaccharide derived from *Amomum villosum* Lour. also possesses a backbone of →4)-α-D-GalAp-(1→ with highly branched side chains (including →3,4)-α-D-GalAp-(1→, →4)-α-D-GalAp-(1→, 6)-α-D-Galp-(1→, and →4)-β-D-Glcp-(1→)[15]. This structural parallel further underscores a highly branched configuration is a critical functional determinant for biological potency. Collectively, the →4)-α-D-GalAp-(1→ backbone of GBP, integrated with its diverse branching patterns and appropriate Mw establishes the structural foundation for its potent antioxidant and gastroprotective efficacy. In terms of pharmacological intervention, GBP represents a paradigm shift compared to OMZ. While OMZ, a PPI, exerts acid-suppressive effects through the irreversible inhibition of the H^+/K^+-ATPase enzyme in gastric parietal cells[8,77], the therapeutic efficacy of GBP is characterized by a pleiotropic, multimodal paradigm. First, as a physicochemical cytoprotectant, GBP forms a structural scaffold on the gastric mucosal interface, shielding the epithelium from ethanol-induced desiccation. Beyond this passive barrier, GBP actively reshapes the biological microenvironment by bolstering endogenous antioxidant enzymes and attenuating the pro-inflammatory cytokine cascade—contrasting the monotargeted specificity of PPIs. Crucially, our findings reveal a unique regulatory dimension of GBP: the reprogramming of the gastric microbiota and its metabolic profile, a feature conspicuously absent in conventional pharmacotherapy. Furthermore, GBP triggers the PI3K/Rac1 signaling axis, which is essential for cytoskeletal reorganization and rapid epithelial restitution. This integrated approach—synergizing physical shielding, biochemical modulation, and microbial homeostasis—suggests that natural polysaccharides like GEP offer a more holistic and robust strategy for preserving mucosal integrity against acute ethanol-induced challenges than targeted enzymatic inhibition.

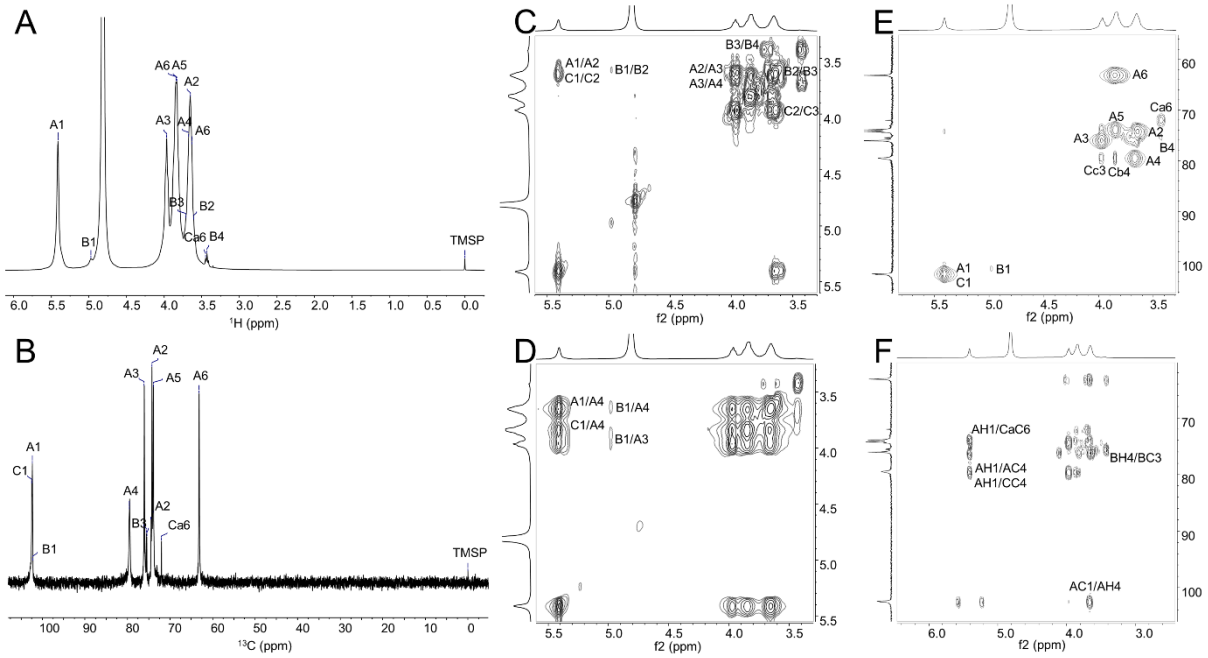

Fig. 8 The NMR spectroscopy of GBP. (A) ^{1}H NMR. (B) ^{13}C NMR. (C) COSY. (D) NOESY. (E) HSQC. (F) HMBC.

4. Conclusion

In conclusion, this study demonstrated the therapeutic potential of GEP in treating ethanol-induced acute gastric mucosal injury in rat models. Notably, GEP-M, GEP-H and GBP exhibited superior efficacy in alleviating gastric mucosal injury symptoms, including hemorrhage, edema, and bleeding. The protective mechanisms operate through multiple pathways (Fig. 9). GEP-M and GBP treatment enhanced the antioxidant defense system by elevating SOD and GSH while reducing MDA levels, thereby protecting gastric mucosal cells from oxidative damage. Furthermore, these polysaccharides restored the gastrointestinal microbiota homeostasis by increasing the abundance of probiotics (such as *Lactobacillus* and *Bifidobacterium*) while reducing the abundance of pathogenic bacteria (such as *Helicobacter*, *Escherichia-Shigella*, and *Streptococcus*). Metabolomic analysis revealed that GEP reversed metabolic disturbances by regulating key pathways, including the TCA cycle, glycolysis, tryptophan metabolism, steroid hormone biosynthesis, and primary bile acid biosynthesis. Microbiota-metabolite interactions emerged as pivotal mediators, with *Bifidobacterium*, *Blautia*, and *Lactobacillus* showing positive correlations with tryptophan metabolites implicated in mucosal repair. To systematically explore the functional connections between these differentially metabolites and signaling pathways, we constructed a metabolite–gene interaction network. This analysis revealed 94 key genes directly associated with differential metabolites, 31 of which underwent transcriptional validation. Subsequent mRNA and protein expression analyses confirmed the activation of the PI3K/Rac1, suggesting its roles in cell proliferation and vascular remodeling during injury resolution. Besides, GBP features a →4)-α-D-Glcp-(1→ backbone with side chains comprising α-D-Glcp-(1→, →4,6)-α-D-Glcp-(1→, →2,4)-α-D-Glcp-(1→, and →3,4)-α-D-Glcp-(1→ units. These findings

comprehensively elucidated that the protective effect of GEP on gastric mucosa injury may be related to its regulation of intestinal flora, thereby influencing the host metabolic profile and ultimately activating the PI3K/Rac1 signaling pathway. This study further provides a material basis and theoretical foundation for the development of *G. elata* polysaccharides-based gastric mucosal protective agents and treating gastric diseases.

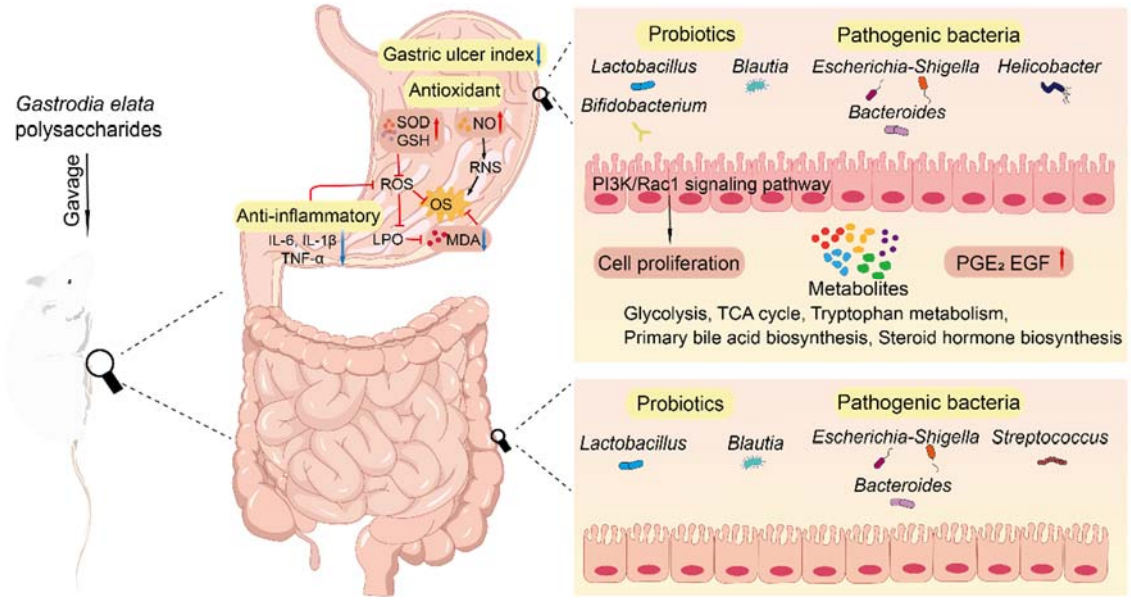

Fig. 9 Potential protective mechanisms of GBP against ethanol-induced gastric mucosal injury. Red arrows indicate significant increase, while blue arrows indicate significant decrease.

Declaration of competing interest

The authors declare no competing financial interests.

Acknowledgment

This research work was supported by the National Natural Science Foundation of China (No. 82104356) and the Fundamental Research Funds for the Central Universities (No. 30924010832). The authors also sincerely thank Open Funding Project of Large Apparatus and equipment (Nanjing University of Science and Technology).

Appendix A. Supplementary data

Supplementary data associated with this article can be found, in the online version, at

References

[1] X. Xia, X. Xu, B. Wang, et.al, Adhesive hemostatic Hydrogel with ultrafast gelation arrests acute upper gastrointestinal hemorrhage in pigs, Adv. Funct. Mater. 32(16) (2022) 2109332. https://doi.org/10.1002/adfm.202109332.

[2] M. Jacome-sosa, Z. Miao, V.S. Peche, et.al, *CD36* maintains the gastric mucosa and associates with gastric disease, Commun. Biol. 4(1) (2021) 1247. https://doi.org/10.1038/s42003-021-02765-z.

[3] Z. Zhou, L. Wang, D. Yang, et.al, Acid-triggered charge-switchable antibacterial hydrogel for accelerated healing of gastric mucosal wounds, ACS Nano 19(18) (2025) 17533-17553. https://doi.org/10.1021/acsnano.5c00426.

[4] K.A. Bockerstett, R.J. Dipaolo, Regulation of gastric carcinogenesis by inflammatory cytokines, Cell. Mol. Gastroenterol. Hepatol. 4 (2017) 47-53. https://doi.org/10.1016/j.jcmgh.2017.03.005.

[5] Y. Teng, R. Xie, J. Xu, et.al, Tubulointerstitial nephritis antigen-like 1 is a novel matricellular protein that promotes gastric bacterial colonization and gastritis in the setting of *Helicobacter pylori* infection, Cell. Mol. Immunol. 20 (2023) 924-940. https://doi.org/10.1038/s41423-023-01055-4.

[6] S.G. Hoft, M. Brennan, J.A. Carrero, et.al, Unveiling Cancer-related metaplastic cells in both *Helicobacter pylori* infection and autoimmune gastritis, Gastroenterology 168 (2025) 53-67. https://doi.org/10.1053/J.GASTRO.2024.08.032.

[7] I. Bjarnason, C. Scarpignato, E. Holmgren, et.al, Mechanisms of damage to the gastrointestinal tract from nonsteroidal anti-inflammatory drugs, Gastroenterology 154 (2018) 500-514. https://doi.org/10.1053/j.gastro.2017.10.049.

[8] Z. Zhang, H. Xie, M.A. Farag, et.al, Dendrobium officinale flowers flavonoids enriched extract protects against acute ethanol-induced gastric ulcers via AMPK/PI3K signaling pathways, Food Sci. Hum. Wellness 13 (2024) 3661-3679. https://doi.org/10.26599/FSHW.2023.9250048.

[9] J.A. Hawley, S.C. Forster, E.M. Giles, Exercise, the gut microbiome and gastrointestinal diseases: therapeutic impact and molecular mechanisms, Gastroenterology 169 (2025) 48-62. https://doi.org/10.1053/j.gastro.2025.01.224.

[10] R. Yang, X. Zhao, W. Wu, et.al, Potential of probiotics for use as functional foods in patients with non-infectious gastric ulcer, Trends Food Sci. Technol. 111 (2021) 463-474. https://doi.org/10.1016/j.tifs.2021.02.070.

[11] X. Yu, J. Ou, L. Wang, et.al, Gut microbiota modulate $CD8^+$ T cell immunity in gastric cancer through Butyrate/GPR109A/HOPX, Gut Microbes 16(1) (2024) 2307542. https://doi.org/10.1080/19490976.2024.2307542.

[12] R. Zeng, H. Gou, H. Cheuk, et.al, Stomach microbiota in gastric cancer development and clinical implications, Gut 73 (2024) 2062-2073. https://doi.org/10.1136/gutjnl-2024-332815.

[13] Y. Li, B. Zhu, T. Chen, et.al, Construction of magnolol nanoparticles for alleviation of ethanol-induced acute gastric injury, J. Agric. Food Chem. 72 (2024) 7933-7942. https://doi.org/10.1021/acs.jafc.3c09902.

[14] Y. Xu, L. Lin, H. Zheng, et.al, Protective effect of amauroderma rugosum ethanol extract and its primary bioactive compound, ergosterol, against acute gastric ulcers based on LXR-mediated gastric mucus secretions, Phytomedicine 123 (2024) 155236. https://doi.org/10.1016/j.phymed.2023.155236.

[15] H. Liu, S. Zhuang, C. Liang, et.al, Effects of a polysaccharide extract from *Amomum villosum Lour*. on gastric mucosal injury and its potential underlying mechanism, Carbohydr. Polym. 294 (2022) 119822. https://doi.org/10.1016/j.carbpol.2022.119822.

[16] L.C. Pereira, F.G. Nascimento, S.R.B.D. Oliveira, et.al, Protective effect against gastric mucosa injury of a sulfated agaran from *Acanthophora spicifera*, Carbohydr. Polym. 261 (2021) 117829. https://doi.org/10.1016/j.carbpol.2021.117829.

[17] X. Wang, J. Yin, M. Zhao, et.al, Gastroprotective activity of polysaccharide from *Hericium erinaceus* against ethanol-induced gastric mucosal lesion and pylorus ligation-induced gastric ulcer, and its antioxidant activities, Carbohydr. Polym. 186 (2018) 100-109. https://doi.org/10.1016/j.carbpol.2018.01.004.

[18] C. Hou, L. Liu, J. Ren, et.al, Structural characterization of two *Hericium erinaceus* polysaccharides and their protective effects on the alcohol-induced gastric mucosal injury, Food Chem. 375 (2022) 131896. https://doi.org/10.1016/j.foodchem.2021.131896.

[19] J. Guan, Z. Chen, L. Guo, et.al, Evaluation of how sulfur-fumigation reduces the edible quality and flavor of *Gastrodia elata* Blume Rhizoma, LWT 187 (2023) 115296. https://doi.org/10.1016/j.lwt.2023.115296.

[20] Z. Chen, L. Li, L. Guo, et.al, A *Gastrodia elata* polysaccharide for restoring intestinal immunocompromise, Int. J. Biol. Macromol. 307 (2025) 141781. https://doi.org/10.1016/j.ijbiomac.2025.141781.

[21] H. Guan, X. Ling, J. Xu, et.al, Structural characterization of polysaccharide derived from *Gastrodia elata* and its immunostimulatory effect on RAW264.7 cells, Molecules 27 (2022) 8059. https://doi.org/10.3390/molecules27228059.

[22] C. Chen, Y. Fu, M. Li, et.al, Nuclear magnetic resonance-based metabolomics approach to evaluate preventive and therapeutic effects of *Gastrodia elata* Blume on chronic atrophic gastritis, J. Pharm. Biomed. Anal. 164 (2019) 231-240. https://doi.org/10.1016/j.jpba.2018.10.035.

[23] D. Xu, Q. Wu, W. Liu, et.al, Therapeutic efficacy and underlying mechanisms of *Gastrodia elata* polysaccharides on dextran sulfate sodium-induced inflammatory bowel disease in mice: modulation of the gut microbiota and improvement of metabolic disorders, Int. J. Biol. Macromol. 248 (2023) 125919. https://doi.org/10.1016/j.ijbiomac.2023.125919.

[24] J. Park, K. Jang, C. Kim, et.al, *Ganoderma Lucidum* pharmacopuncture for teating ethanol-induced chronic gastric ulcers in rats, J. Pharmacopuncture 18 (2015) 72-78. https://doi.org/10.3831/KPI.2014.18.008.

[25] Q. Xu, R. Gan, Q. Wang, et.al, Metabolomic and molecular analysis reveals multiple pathways of TBBPA-induced developmental toxicity in zebrafish embryos, Toxicol. Appl. Pharmacol. 498 (2025) 117295. https://doi.org/10.1016/j.taap.2025.117295.

[26] Z. Hu, D. Xu, H. Meng, et.al, 4-octyl itaconate protects against oxidative stress-induced liver injury by activating the Nrf2/Sirt3 pathway through AKT and ERK1/2 phosphorylation, Biochem. Pharmacol. J. 220 (2024) 115992. https://doi.org/10.1016/j.bcp.2023.115992.

[27] T. Yu, H. Zhang, J. Xie, et.al, Deciphering the toxicological mechanisms of per- and polyfluoroalkyl substances (PFAS) in musculoskeletal disorders via integrated network toxicology and molecular docking, Environ. Int. 206 (2025) 109934. https://doi.org/10.1016/j.envint.2025.109934.

[28] S. Chen, R. Cheng, X. Xu, et.al, The structure and flocculation characteristics of a novel exopolysaccharide from a Paenibacillus isolate, Carbohydr. Polym. 291 (2022) 119561. https://doi.org/10.1016/j.carbpol.2022.119561.

[29] H. Matsui, Y. Nagano, O. Shimokawa, et.al, Gastric acid induces mitochondrial superoxide production and lipid peroxidation in gastric epithelial cells, J. Gastroenterol. 46 (2011) 1167-1176. https://doi.org/10.1007/s00535-011-0434-6.

[30] S. Verma, V.L. Kumar, Attenuation of gastric mucosal damage by artesunate in rat: modulation of oxidative stress and NFκB mediated signaling, Chem. Biol. Interact. 257 (2016) 46-53. https://doi.org/10.1016/j.cbi.2016.07.027.

[31] A. Bansal, M.C. Simon, Glutathione metabolism in cancer progression and treatment resistance, J. Cell Biol. 217 (2018) 2291-2298. https://doi.org/10.1083/jcb.201804161.

[32]L. Kennedy, J.K. Sandhu, M. Harper, Role of glutathione in cancer: from mechanisms to therapies, Biomolecules. 10(10) (2020) 1429. https://doi.org/10.3390/biom10101429.

[33] J. Mu, C. Li, Y. Shi, et.al, Protective effect of platinum nano-antioxidant and nitric oxide against hepatic ischemia-reperfusion injury, Nat. Commun. 13(1) (2022) 2513. https://doi.org/10.1038/s41467-022-29772-w.

[34] R. Akanda, B. Park, Involvement of MAPK/NF-κB signal transduction pathways: camellia japonica mitigates inflammation and gastric ulcer, Biomed. Pharmacother. 95 (2017) 1139-1146. https://doi.org/10.1016/j.biopha.2017.09.031.

[35] S. Lu, S. Kong, Y. Wang, et.al, Gastric acid-response chitosan/alginate/tilapia collagen peptide composite hydrogel: protection effects on alcohol-induced gastric mucosal injury, Carbohydr. Polym. 277 (2022) 118816. https://doi.org/10.1016/j.carbpol.2021.118816.

[36] S. Wölf, A.A. Daddi, A. Imai-matsushima, et.al, EGF and BMPs govern differentiation and patterning in human gastric glands, Gastroenterology 161 (2021) 623-636.e36. https://doi.org/10.1053/j.gastro.2021.04.062.

[37] K. Li, X. Ma, Z. Li, et.al, A natural peptide from a traditional Chinese medicine has the potential to treat chronic atrophic gastritis by activating gastric stem cells, Adv. Sci. 2304326 (2024) 1-15. https://doi.org/10.1002/advs.202304326.

[38] R. Zhao, S. Hu, Z. Yang, et.al, Targeted quercetin delivery nanoplatform via folic acid-functionalized metal-organic framework for alleviating ethanol-induced gastric ulcer, Chem. Eng. J. 498 (2024) 155700. https://doi.org/10.1016/j.cej.2024.155700.

[39] W. Chen, D. Wu, Y. Jin, et.al, Pre-protective effect of polysaccharides purified from *Hericium erinaceus* against ethanol-induced gastric mucosal injury in rats, Int. J. Biol. Macromol. 159 (2020) 948-956. https://doi.org/10.1016/j.ijbiomac.2020.05.163.

[40] H. Gong, D. Han, Z. Luo, et.al, Xiangshao Decoction alleviates gastric mucosal injury through NRF2 signaling pathway and reduces neuroinflammation in gastric ulcer rats, Phytomedicine 118 (2023) 154954. https://doi.org/10.1016/j.phymed.2023.154954.

[41] Z. Zheng, N. Sun, J. Yang, et.al, Sea cucumber gut tetrapeptide ameliorates alcoholic gastric damage via restoring mitochondrial dynamics, Food Sci. Hum. Wellness 14 (2025) 9250183. https://doi.org/10.26599/FSHW.2024.9250183.

[42] B. Ezraty, A. Gennaris, F. Barras, et.al, Oxidative stress, protein damage and repair in bacteria, Nat. Rev. Microbiol. 15(7) (2017) 385-396. https://doi.org/10.1038/nrmicro.2017.26.

[43] R. Okumura, K. Takeda, Maintenance of intestinal homeostasis by mucosal barriers, Inflamm. Regen. 38 (2018) 5. https://doi.org/10.1186/s41232-018-0063-z.

[44] M.E. V Johansson, H. Sjövall, G.C. Hansson, The gastrointestinal mucus system in health and disease, Nat. Rev. Gastroenterol. Hepatol. 10 (2013) 352-361. https://doi.org/10.1038/nrgastro.2013.35.

[45] S. Kumar, D.C. Metz, S. Ellenberg, et.al, Risk factors and incidence of gastric cancer after detection of *Helicobacter pylori* infection: a large cohort study, Gastroenterology 158 (2020) 527-536.e7. https://doi.org/10.1053/j.gastro.2019.10.019.

[46] P. Malfertheiner, M.C. Camargo, E. El-omar, et.al, *Helicobacter pylori* infection, Nat. Rev. Dis. Prim. 9 (2023) 19. https://doi.org/10.1038/s41572-023-00431-8.

[47] W. Zhang, Y. Zhou, Y. Fan, et.al, Metal-organic-framework-based hydrogen-release platform for multieffective *Helicobacter pylori* targeting therapy and intestinal flora protective capabilities, Adv. Mater. 34(2) (2022) e2105738. https://doi.org/10.1002/adma.202105738.

[48] H. Ge, F. Qi, Z. Shen, et.al, Large-leaf yellow tea protein derived-peptides alleviated dextran sodium sulfate-induced acute colitis and restored intestinal microbiota balance in C57BL/6 J mice, Food Chem. 456 (2024) 139936. https://doi.org/10.1016/j.foodchem.2024.139936.

[49] A. Nabavi-rad, A. Sadeghi, H. Asadzadeh, et.al, The double-edged sword of probiotic supplementation on gut microbiota structure in *Helicobacter pylori* management, Gut Microbes 14 (2022) 1-34. https://doi.org/10.1080/19490976.2022.2108655.

[50] X. Liu, B. Mao, J. Gu, et.al, *Blautia*-a new functional genus with potential probiotic properties?, Gut Microbes 13 (2021) 1-21. https://doi.org/10.1080/19490976.2021.1875796.

[51] Y. Guo, Y. Zhang, M. Gerhard, et.al, Effect of *Helicobacter pylori* on gastrointestinal microbiota: a population-based study in Linqu , a high risk area of gastric cancer, Gut 69(9) (2020) 1598-1607. https://doi.org/10.1136/gutjnl-2019-319696.

[52] O.O. Coker, Z. Dai, Y. Nie, et.al, Mucosal microbiome dysbiosis in gastric carcinogenesis, Gut 67(6) (2018) 1024-1032. https://doi.org/10.1136/gutjnl-2017-314281.

[53] X. Ren, J. Ma, Y. Dong, et.al, Discovery of active compounds and key targets of *Thymus quinquecostatus* Celak. based on gastrointestinal metabolism and Gut flora-Compound-Target-Pathway network with TOPSIS method, Food Sci. Hum. Wellness 14 (2025) 9250273. https://doi.org/10.26599/FSHW.2024.9250273.

[54] T. Chen, J. Chen, S. Bao, et.al, Mechanism of Xiaojianzhong decoction in alleviating aspirin-induced gastric mucosal injury revealed by transcriptomics and metabolomics, J. Ethnopharmacol. 318 (2024) 116910. https://doi.org/10.1016/j.jep.2023.116910.

[55] C. Becker, T.E. Adolph, Disentangling tryptophan metabolism in inflammatory bowel diseases, Gut 72(7) (2023) 1235-1236. https://doi.org/10.1136/gutjnl-2022-328853.

[56] D.M.M. Harris, S. Szymczak, S. Schuchardt, et.al, Tryptophan degradation as a systems phenomenon in inflammation-an analysis across 13 chronic inflammatory diseases, EBioMedicine 102 (2024) 105056. https://doi.org/10.1016/j.ebiom.2024.105056.

[57] E. Urbauer, D. Aguanno, N. Mindermann, et.al, Mitochondrial perturbation in the intestine causes microbiota-dependent injury and gene signatures discriminative of inflammatory disease, Cell Host Microbe 32(8) (2024) 1347-1364.e10. https://doi.org/10.1016/j.chom.2024.06.013.

[58] C. Fenton, C. Martin, R. Jones, et.al, Local steroid activation is a critical mediator of the anti-inflammatory actions of therapeutic glucocorticoids, Ann. Rheum. Dis. 80(2) (2020) 250-260. https://doi.org/10.1136/annrheumdis-2020-218493.

[59] W. Jing, S. Dong, Y. Xu, et.al, Gut microbiota-derived tryptophan metabolites regulated by Wuji Wan to attenuate colitis through AhR signaling activation, Acta Pharm. Sin. B 15(1) (2025) 205-223. https://doi.org/10.1016/j.apsb.2024.11.009.

[60] K. Peuker, S. Muff, J. Wang, et.al, Epithelial calcineurin controls microbiota-dependent intestinal tumor development, Nat. Med. 22 (2016) 506-515. https://doi.org/10.1038/nm.4072.

[61] L. Wang, X. Mao, X. Yu, et.al, *FPR3* reprograms glycolytic metabolism and stemness in gastric cancer via calcium-NFATc1 pathway, Cancer Lett. 593 (2024) 216841. https://doi.org/10.1016/j.canlet.2024.216841.

[62] J. Massagué, D. Sheppard, TGF-β signaling in health and disease, Cell 186(19) (2023) 4007-4037. https://doi.org/10.1016/j.cell.2023.07.036.

[63] M. Maldonado, S. Dharmawardhane, Targeting *rac* and *cdc42* GTPases in cancer, Cancer Res. 78(12) (2018) 3101-3111. https://doi.org/10.1158/0008-5472.CAN-18-0619.

[64] L. Cao, S. Zhu, H. Lu, et.al, *Helicobacter pylori*-induced RASAL2 through activation of nuclear Factor-κB promotes gastric tumorigenesis via β-catenin signaling axis, Gastroenterology 162(6) (2022) 1716-1731.e17. https://doi.org/10.1053/j.gastro.2022.01.046.

[65] S. Yan, S. Bao, T. Chen, et.al, Cinnamaldehyde alleviates aspirin-induced gastric mucosal injury by regulating pi3k/akt pathway-mediated apoptosis, autophagy and ferroptosis, Phytomedicine 132 (2024) 155791. https://doi.org/10.1016/j.phymed.2024.155791.

[66] Y. Zeng, M. Ren, Y. Li, et.al, Knockdown of RhoGDI2 represses human gastric cancer cell proliferation, invasion and drug resistance via the Rac1/Pak1/LIMK1 pathway, Cancer Lett. 492 (2020) 136-146. https://doi.org/10.1016/j.canlet.2020.07.013.

[67] Z. Lv, M. Hu, M. Fan, et.al, Podocyte-specific *Rac1* deficiency ameliorates podocyte damage and proteinuria in STZ-induced diabetic nephropathy in mice, Cell Death Dis. 9(3) (2018) 342. https://doi.org/10.1038/s41419-018-0353-z.

[68] F. Yu, C. Yu, F. Li, et.al, Wnt/β-catenin signaling in cancers and targeted therapies, Signal Transduct. Target. Ther. 6(1) (2021) 307. https://doi.org/10.1038/s41392-021-00701-5.

[69] C. Liu, S. Chen, Y. Zhang, et.al, Mechanisms of Rho GTPases in regulating tumor proliferation, migration and invasion, Cytokine Growth Factor Rev. 80 (2024) 168-174. https://doi.org/10.1016/j.cytogfr.2024.09.002.

[70] Y. Qian, X. Liang, P. Kong, et.al, Elevated DHODH expression promotes cell proliferation via stabilizing *β-catenin* in esophageal squamous cell carcinoma, Cell Death Dis. 11(10) (2020) 862. https://doi.org/10.1038/s41419-020-03044-1.

[71] L. Pan, L. Wang, Z. Zeng, et.al, Chemical structure and prebiotic activity of a *Dictyophora indusiata* polysaccharide fraction, Food Chem. 463 (2025) 141086. https://doi.org/10.1016/j.foodchem.2024.141086.

[72] X. Xu, D. Shi, L. Xu, et.al, Unveiling the structural characteristics and anti-inflammatory potential of a novel polysaccharide from sweet potato peels, Food Biosci. 62 (2024) 105375. https://doi.org/10.1016/j.fbio.2024.105375.

[73] Z. Zhu, C. Chen, H. Sun, et.al, Structural characterisation and ACE-inhibitory activities of polysaccharide from *Gastrodia elata* Blume, Nat. Prod. Res. 33 (2018) 1721-1726. https://doi.org/10.1080/14786419.2018.1434643.

[74] J. Chen, S. Tian, X. Shu, et.al, Extraction, characterization and immunological activity of polysaccharides from *Rhizoma gastrodiae*, Int. J. Mol. Sci. 17 (2016) 1011. https://doi.org/10.3390/ijms17071011.

[75] X. Wang, M. Wang, J. Yin, et.al, Gastroprotective activity of polysaccharide from the fruiting body of *Hericium erinaceus* against acetic acid-induced gastric ulcer in rats and structure of one bioactive fraction, Int. J. Biol. Macromol. 210 (2022) 455-464. https://doi.org/10.1016/j.ijbiomac.2022.04.153.

[76] H. Hui, X. Li, H. Jin, et.al, Structural characterization, antioxidant and antibacterial activities of two heteropolysaccharides purified from the bulbs of *Lilium davidii* var. unicolor Cotton, Int. J. Biol. Macromol. 133 (2019) 306-315. https://doi.org/10.1016/j.ijbiomac.2019.04.082.

[77] P. Malfertheiner, A. Kandulski, M. Venerito, Proton-pump inhibitors: understanding the complications and risks, Nat. Rev. Gastroenterol. Hepatol. 14 (2017) 697-710. https://doi.org/10.1038/nrgastro.2017.117.